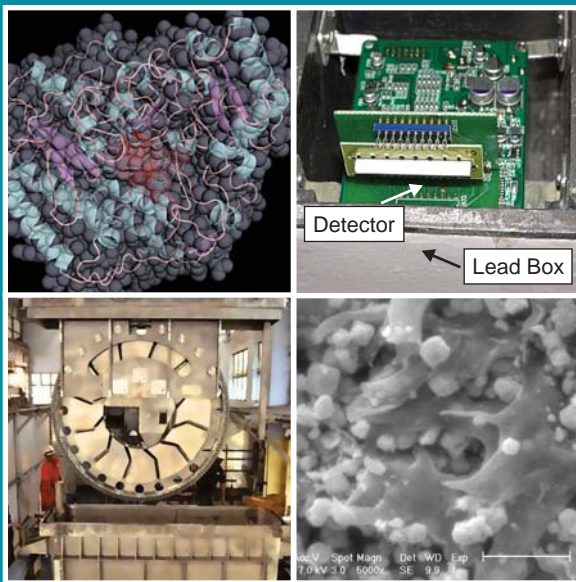


BARC

NEWSLETTER



भाभा परमाणु अनुसंधान केंद्र
BHABHA ATOMIC RESEARCH CENTRE



IN THIS ISSUE

- Bioremediation: Discovery of a Novel Alkaline Phosphatase through X-ray Crystallography
- Improved Location of Earthquakes in Sumatra Region using Gauribidanur Seismic Array Data
- DNA Repair and Recombination Proteins (Dmc1 and Rad51) from Rice (*Oryza Sativa*)
- Recovery of Cesium from High Level Liquid Nuclear Waste by an Advanced Polymer Composite
- Performance Study of Indigenously Developed CsI-Photodiode Linear Array Detectors for X-Ray Baggage Scanning Application
- Marx Generator and Reflex Triode based High Power Pulsed



In the Forthcoming Issue

1. **Genetic Analysis of Type2 Diabetes**
Suresh KG Shettigar et al.
2. **Advanced Research on Master Curve for Integrity Assessment of Reactor Pressure Vessel**
J. Chattopadhyay et al.
3. **Design, Development and Deployment of Special Sealing Plug for 540 MWe PHWRs**
G. Sharma et al.
4. **Decontamination of Alpha Contaminated Metallic Waste by Cerium IV Redox Process**
J.G. Shah
5. **Non-invasive Blood Pressure Monitor; Beat to Beat**
Vineet Sinha et al.
6. **Self Assembled Systems: Design and Drug Delivery Perspectives**
Gunjan Verma et al.

CONTENTS

<i>Editorial Note</i>	II
Brief Communication	
• Integrated Δ -E Silicon Detector Telescope	III
• Development of Continuous Rotary Dissolver	IV
• Design and Development of Metallic Face Seal for AHWR Fuelling Machine	V
• Meso-and B-substituted Pyrromethene Fluorophores as New Photo-stable Laser Dyes	VI
• Ultra High Precision Wave Length Scanning Mechanism	VII
• Evaluation of Tripodal / Calixarene Based Diglycolamides for Actinide Extraction	VIII
Focus	
• Discovery of Higgs Boson: The God Particle <i>Ajit Kumar Mohanty</i>	1
Research Articles	
• Bioremediation: Discovery of a novel alkaline phosphatase through X-ray crystallography <i>Subhash C. Bihani, Shree Kumar Apte, Jean-Luc Ferrer and Madhusoodan V. Hosur</i>	6
• Improved Location of Earthquakes in Sumatra Region using Gauribidanur Seismic Array Data <i>Manoj Kumar and Falguni Roy</i>	15
Technology Development Articles	
• DNA Repair and Recombination Proteins (Dmc1 and Rad51) from Rice (<i>Oryza sativa</i>) <i>Rajani Kant Chittela and Jayashree K. Sainis</i>	21
• Recovery of Cesium from High Level Liquid Nuclear Waste by an Advanced Polymer Composite <i>Lalit Varshney, V. Venugopal et al.</i>	26
Feature Articles	
• Performance Study of Indigenously Developed CsI-Photodiode Linear Array Detectors for X-Ray Baggage Scanning Application <i>Anita Topkar, Arvind Singh, P.K. Mukhopadhyay, et al.</i>	31
• Marx Generator and Reflex Triode based High Power Pulsed Microwave Source <i>Archana Sharma, Amitava Roy, Sabyasachi Mitra, et al.</i>	37
News and Events	
• Technology Transfers from BARC	43
• BRNS-AEACI Third School on Analytical Chemistry (SAC-3): a Report	46
• Technology of Indigenous Digital Radiotherapy Simulator Transferred	48
• Graduation Day Function of the BARC Training School; a Report	49
• National Fire Service Week at BARC: a Report	50
• Release of BARC Logo and Launching of an Enhanced Website for BARC: a Report	51
• Nuclear Energy and Development of Country (NEDC – 2012): a Report	52
BARC Scientists Honoured	

Editorial Committee**Chairman**

Dr. Tulsi Mukherjee,
Director, Chemistry Group

Vice Chairman

Dr. N. Ramamoorthy,
Senior Advisor to Director, BARC

Edited by

Dr. K. Bhanumurthy
Head, SIRD

Associate Editors for this issue

Dr. G. Rami Reddy, RSD
Dr. A. Vinod Kumar, EAD
Mr. Avaneesh Sharma, RED

Members

Dr. Tulsi Mukherjee
Dr. N. Ramamoorthy
Dr. D.N. Badodkar, DRHR
Dr. A.P. Tiwari, RCnD
Dr. Madangopal Krishnan, MSD
Dr. A.K. Tyagi, CD
Dr. P.V. Varde, RRSD
Dr. S.M. Yusuf, SSPD
Mr. Avaneesh Sharma, RED
Dr. C. Srinivas, PsDD
Dr. G. Rami Reddy, RSD
Dr. S.K. Mukherjee, FCD
Mr. G. Venugopala Rao, APPD
Dr. A. Vinod Kumar, EAD
Dr. Anand Ballal, MBD
Dr. K. Bhanumurthy, SIRD
Dr. S.C. Deokathey, SIRD

From the Editor's Desk

This issue of the BARC Newsletter is special. For the first time, the BARC Newsletter proudly carries the BARC logo on the front cover. The BARC logo was officially released on 10th August, 2012 by Shri Sekhar Basu, Director, BARC. On the same day, he also launched the enhanced website of BARC showcasing several new and attractive features.

We would like to thank all our Scientists and Engineers for their response to the uploading of Award winning articles for the Founder's Day Special Issue of the BARC Newsletter. This year we received a total of 64 papers which will be released in the form of a CD on Founder's Day.

On 4th July 2012, the CMS and the ATLAS experimental teams at CERN announced the discovery of the Higg's Boson, a landmark event in the field of Particle Physics. We carry a special feature on this important event and BARC's contribution in this exciting area. Apart from this, six articles on diverse areas of R&D in BARC are covered in the issue.

We would like to inform you that the "Brief Communications" Section, introduced this year, has attracted the attention of several scientists and engineers. In order to further strengthen the BARC Newsletter, it is necessary that contributions come from various divisions and it is our experience that feature articles written in simplified format attract large readership.



Dr. K. Bhanumurthy
On behalf of the Editorial Committee

Integrated Δ -E Silicon Detector Telescope

(Electronics & Instrumentation Group)

Particle identification method using E- Δ E detector telescope is extensively used in physics experiments. For heavy ions and fission fragments, the Δ E detector of the telescope needs to have a thickness of a few microns which is difficult to attain using conventional silicon machining process. Conventional Δ E detectors are also very fragile, and this puts serious limitation to their applications for multi detector array system. To overcome these limitations, a novel silicon detector telescope for particle identification and measurement of their energy has been developed. The thin Δ E and thick E detectors are integrated on the same silicon chip. Δ E is fabricated on the front side and E detector on the back side of the wafer, with a common buried contact. The detector is fabricated using a complex process sequence involving double sided silicon wafer processing (Fig. 1 & Fig. 2). These detectors are rugged to handle and could be used in multi-detector systems. Also, Δ E detectors with a thickness of a few microns and larger area of 100mm² or more can be fabricated using this technology. Such integrated E- Δ E detector telescopes are not commercially available. The performance of this detector has been investigated in collaboration with NPD and demonstrated to be as good as conventional telescope incorporating physically separate Δ E and E imported silicon detectors. Presently, detectors with Δ E thicknesses of 10 μ m, 15 μ m, and 25 μ m, and E detector of thickness 300 μ m have been developed. This integrated detector telescope (Fig. 3) could also find interesting applications in neutron spectrometry and medical dosimetry with good n/g discrimination. The detector design and technology can be adopted to fabricate segmented detector telescopes which could also identify the position of particles in addition to particle identification and energy measurement.

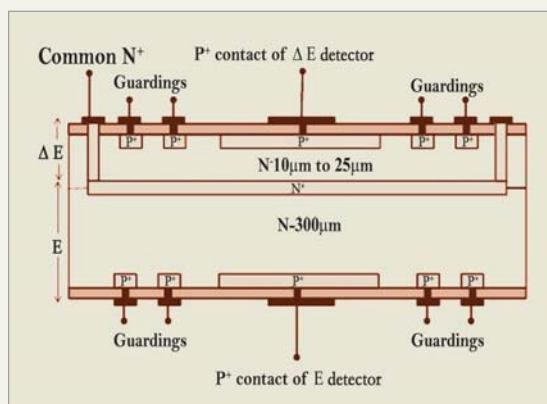


Fig.1: Schematic cross section of the Δ E-E detector

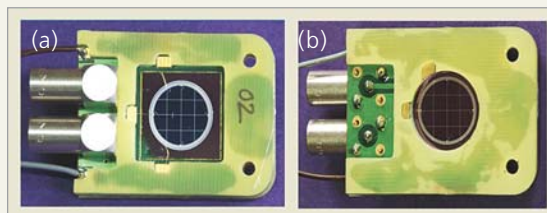


Fig.2 : Front side Δ E and b) back side E detector

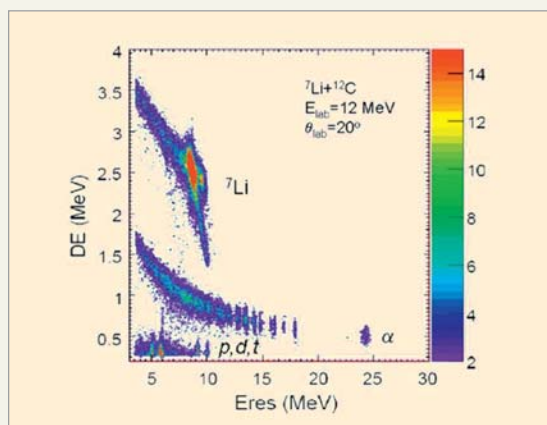


Fig.3: A two dimensional spectrum obtained from the integrated Δ E-E telescope. Different reaction products are identified and labeled [1].

Ref:

[1] A. Topkar et al, "Development of integrated Δ E-E silicon detector telescope using silicon planar technology", *Nucl. Instr. and Meth*, A 654 (2011) 330-335.

Development of Continuous Rotary Dissolver (CRD)

(Nuclear Recycle Group)

Development of continuous dissolution equipment was initiated to meet the requirements of large capacity reprocessing plants. In batch dissolution process, which is presently employed in Indian reprocessing plants, various steps such as charging of chopped fuel, acid addition, dissolution, solution cooling, product filtration cum transfer, hull rinsing cum discharge, and repositioning of basket are carried out sequentially. These sequential operations limit the capacity of the system. In continuous mode of dissolution, these steps are carried out simultaneously and thereby, relatively higher throughput can be achieved. The CRD being developed is based on a bucket wheel assembly with 12 perforated buckets under indexing motion within a slab tank partially filled with nitric acid (Figs. 1 and 2). The chopped fuel pieces are fed to a bucket when it is in the loading position (position 1 in Fig. 1); the wheel is indexed every hour; the fuel pellets dissolve in the acid bath while the bucket is immersed in the acid bath (positions 1 - 4) and the hulls are discharged into the outlet when bucket emerges out of acid and attains unloading position (position 7). A plant scale CRD which was fabricated and tested successfully is undergoing experimental trials. A mathematical model was developed for the dissolution of UO_2 pellets. The model was subsequently used to identify the best mode of operation of the CRD. Different modes considered for the process simulation are: cross current, co-current and counter current flows of acid with respect to the pellet movement. The model predictions show that counter current scheme can process 67.5 kg/h of uranium metal equivalent to a plant throughput of 400 tonnes per year. A test loop is being set up for the performance evaluation of the CRD.

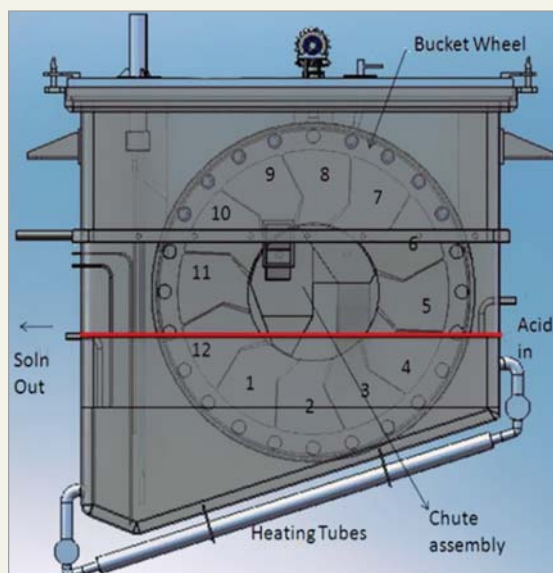


Fig. 1 Conceptual scheme of CRD



Fig. 2 Plant scale CRD during installation

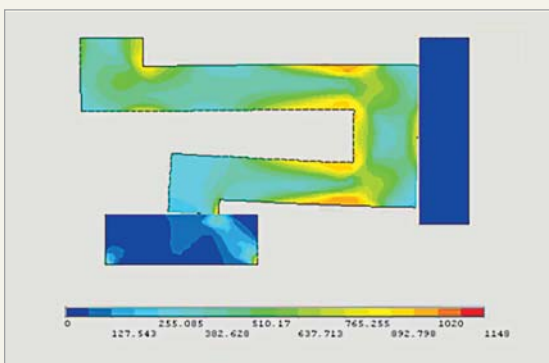
Design and Development of Metallic Face Seal for AHWR Fuelling Machine

(Reactor Design & Development Group)

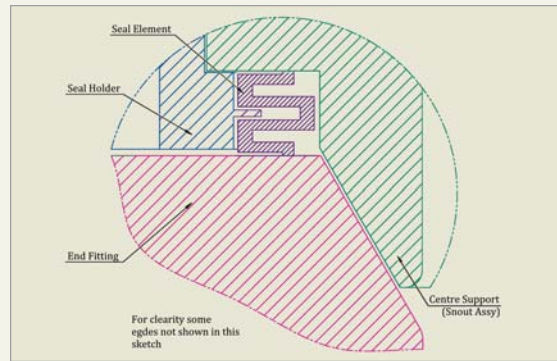
Advanced Heavy Water Reactor (AHWR) is a vertical pressure tube type reactor. A shielded vertical Fuelling Machine (FM) is employed for on/off power refuelling. Coolant channel shall be frequently approached by Fuelling Machine for refuelling operation. A metallic face seal is required between FM and End-Fitting butting faces to maintain leak tightness during refuelling operation. It is an important component as it acts as pressure boundary and prevents the escape of water from the snout cavity.

Efforts are made to develop the component indigenously as an import substitute. Refuelling Technology Division, BARC has developed and qualified the seal for reactor use.

Metallic face seal is a critical component which has been designed to meet the strength as well as flexibility requirements. Basic design of seal was done considering fatigue analysis based on strain cycling, contact stress in the sealing face, self-energizing philosophy and stress consideration. Inconel X-750 material has been chosen to satisfy the variety of requirements like strength at high temperature, good corrosion resistance, excellent spring back characteristics etc. The seal is qualified as per ASME Section III Div. 1 class NB code.



Stress Intensity plot of Metallic Face Seal



Metallic Face Seal in assembled condition

Considering the stringent requirements of seal design, a prototype was manufactured to prove the design. With the help of private firm, manufacturing technology for metallic face seal was developed indigenously. Surface finish of 0.1 micron at the sealing face was achieved by lapping. Groove size as indicated in the drawing was achieved with the help of special diamond grinding wheel of thickness 0.4 mm.

The Metallic Face Seal was tested for the performance in simulated conditions of reactor temperature and pressure. Extensive test program was carried out to qualify the component at high pressure (85 bar) and high temperature (285°C) condition. In order to measure minute leakage at hot condition, a bubble monitoring system was connected to the hydraulic circuit. No leakage was



Metallic Face Seal Test-setup

observed throughout the test. Performance of the seal was found to be satisfactory.

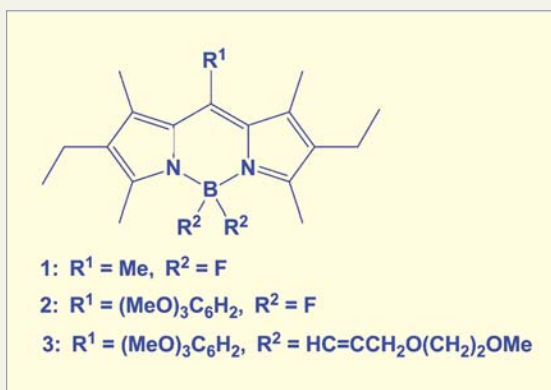
S/Shri G. Sharma, K.K. Jha, K.K. Verma, P. Halder and R.J. Patel contributed in this development work.

Meso- and B-Substituted Pyrromethene Fluorophores as New Photo-stable Laser Dyes

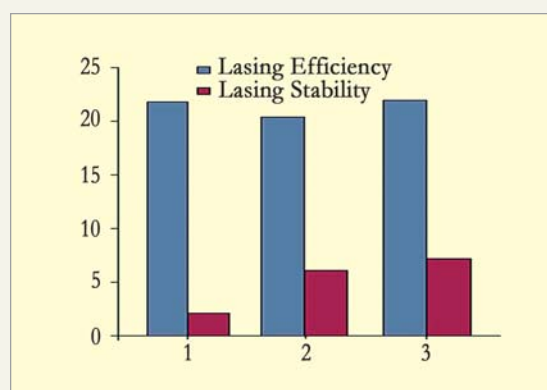
(Chemistry Group)

Dye lasers are one of the most versatile laser sources known today due to their significant contribution to basic physics, chemistry, biology, laser technology, isotope enrichment and other fields. Compared to inorganic lasers the organic dye lasers cover the entire visible and near IR region and have far greater tunability. The pyrromethene (PM) compounds have become the laser dyes of choice to the laser scientists, due to their high fluorescence yields, intense absorption profiles at the green spectral region, low triplet-triplet extinction coefficients over the entire fluorescence region, and excellent lasing efficiency. But their use, particularly in high-repetition-rate liquid dye lasers remains limited owing to rapid photochemical degradation under aerobic conditions. The degradation of the PM dyes is primarily mediated by their *in situ*

reaction with singlet oxygen (1O_2), generated during photochemical excitation. Hence, two new PM compounds were rationally designed and synthesized by attaching an electron rich aryl substitution at C-8 (*meso*) position (dye 2) as such, or in combination with replacement of the F atoms at the B-centre with a judiciously chosen 2,5-dioxaoctyne appendage (dye 3). The new dyes showed equivalent lasing property as that of the commercial PM-567 dye (1), but showed greater photo-chemical stability as shown below. The appendage at the B-centre was particularly useful in imparting better solubility in polar solvents like ethanol, as is required for laser applications.



Chemical structures of the laser dyes



Lasing performance & stability of new PM dyes 2&3

Ultra High Precision Wave Length Scanning Mechanism

(Design, Manufacturing and Automation Group)

BARC has developed a P.C. based “Ultra High Precision Wavelength Scanning Mechanism” which will be used for fine tuning the narrow bandwidth, tunable SLM dye laser. Tuning range of wavelength for the specified purpose is from 559.75556 nm to 559.74642 nm. Tuning in such a narrow bandwidth requires rotational resolution in the range of 0.02 arc-second or better.

A standard rotary table available is driven by a worm and worm gear and the absolute accuracy of the angle is about 0.1 arc second. However in synchrotron and laser beam instruments rotary stages are required with a resolution of one hundredth of a second or better.

In this design, required resolution has been achieved by indirect drive. This rotary table has two stages of drive (Fig. 1). In the first stage 50,000 micro-step stepper motor is directly mounted, which gives 26 arc-second resolution. Second stage drive is a indirect drive. In indirect drive rotary motion is transferred to the rotary table by a set of higher and lower pairs (Fig. 1) with respect to first stage. This design has been adopted for design of ultra high precision rotary mechanism. This high-resolution rotary mechanism is used to rotate the optical elements like grating, mirror, etc with a resolution of 10^{-2} arc-second. The resolution can be increased to 4 milliarcsecond by using piezotransducers in the second stage instead of cam follower. The total range of the instrument is $\pm 13^\circ$. Tuning range of the instrument was observed to be 556.4-568.5 nm. The assembly is



Fig. 1: Assembly with optical mounts

very compact and is universally mountable. This table consists of the following sub-assemblies :

1. First Stage (Coarse) Rotational Mechanism Sub-assembly.
2. Fine Rotational Mechanism Sub-assembly.
3. Base Mount Sub-assembly.
4. Optical Mount Sub-assembly.

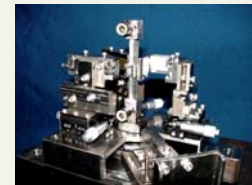


Fig. 2: Arrangement of tuning mirror grating, etc.

Mounting arrangement for optical elements were also design and developed to match the accuracy of rotary table (Fig.2). Here all mounting arrangements are rigid with fine adjustment facility (manually). Mounting arrangements are based on flexural design with micro adjustment facility. Range of angular adjustment is $\pm 2^\circ$ with a resolution of 10 arc sec. Each mount has two such types of unit mounted in perpendicular direction for adjustments in two directions.

Using this technique of rotational mechanism and arrangement of tuning mirror, grating and end mirror in a particular geometric fashion (Fig. 3), mode hop free tuning over the wavelength range ~ 70 GHz was achieved in a single hop mode dye laser. Minimum frequency change for coarse and fine tuning was 39 GHz and 3 MHz, respectively, which was experimentally validated.

This mechanism can also be used as a goniometer and for metrological requirements.

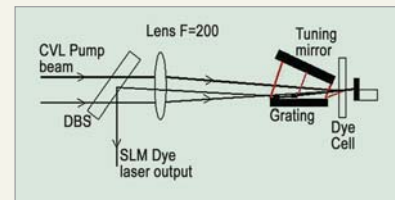


Fig. 3: Schematic of SLM GIG dye laser

Evaluation of Tripodal / Calixarene Based Diglycolamides for Actinide Extraction

(Radiochemistry and Isotope Group)

Diglycolamides (DGA) have been found to be one of the most efficient reagents for trivalent minor actinide extraction from acidic feeds. They act as tridentate ligands due to the presence of an additional oxygen atom between the carbonyl groups, and therefore display a very high affinity toward actinides and lanthanides as compared to other malonamides. In order to enhance their extraction efficiency, several DGA grafted ligands viz., tripodal diglycolamide (T-DGA, Fig. 1(a)) and calix[4]arene DGA (calix-DGA, Fig. 1(c)) were synthesized and evaluated for actinide extraction and supported liquid membrane transport behaviour. Extraction studies with T-DGA for actinide ions such as UO_2^{2+} , Np(IV), Pu(IV), and Am(III) and fission product ions such as Cs^+ and Sr^{2+} from acidic feed solutions indicated exceptionally high D values with Am(III) and Pu(IV) with about 30 times lower concentration of T-DGA (as compared to TODGA (Fig. 1(b)), a well known DGA based extractant being proposed for 'actinide partitioning'). Similar observations were made for the calix-DGA compounds appended with four DGA moieties though the extraction efficiencies for the calix-DGAs were even better than the T-DGA molecule. Typically, for 1 mM extractant concentration and 3 M HNO_3

as the feed acidity, the distribution ratios for Am(III) were about <0.1 , 40 and >300 for TODGA, T-DGA and calix-DGA, respectively. The role of spacer length and substituent effect in the calix-DGA were also investigated and were found to be encouraging for trivalent actinide extraction.

Room temperature ionic liquids containing diglycolamide extractants have shown exceptionally high distribution coefficients and the results indicate possibility of selective recovery of Am from acidic waste solutions. A solvent containing Calix-DGA in room temperature ionic liquids gave exceptionally high separation factor for Am(III) and U(VI). Task specific ionic liquids containing DGA functional groups (Fig. 1(d)) have also been evaluated for actinide extraction under varying experimental conditions and were found to be the most efficient extractant for minor actinides from acidic feed conditions, reported so far. The D_{Am} and D_{Eu} values were 2.2×10^3 and 1.1×10^4 , respectively for 3 M HNO_3 as the feed with separation factor ($D_{\text{Eu}}/D_{\text{Am}}$) values ~ 5 . Stripping and significantly high radiation stability make the DGA functionalized task specific ionic liquids promising alternatives to solvent containing molecular diluents.

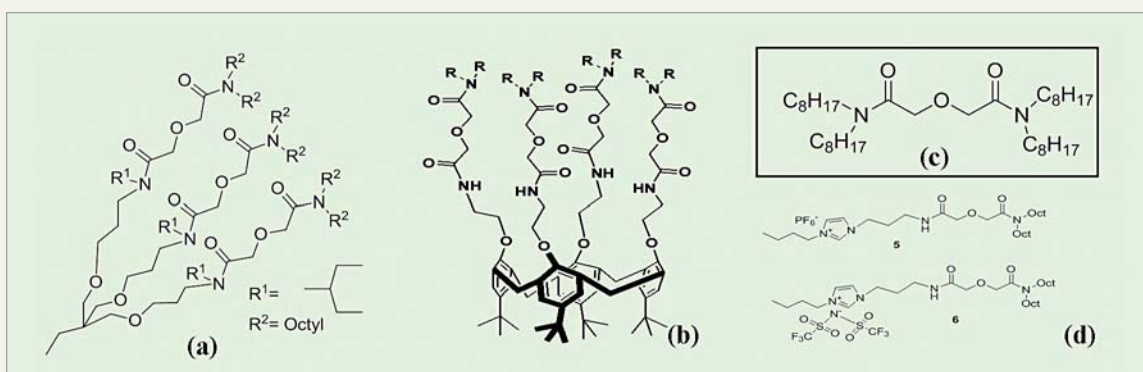


Fig.1: Structures of DGA compounds: (a) T-DGA, (b) TODGA, (c) calix-DGA, (d) Task specific ionic liquids with DGA functional groups

Discovery of Higgs Boson: The God Particle

Ajit Kumar Mohanty

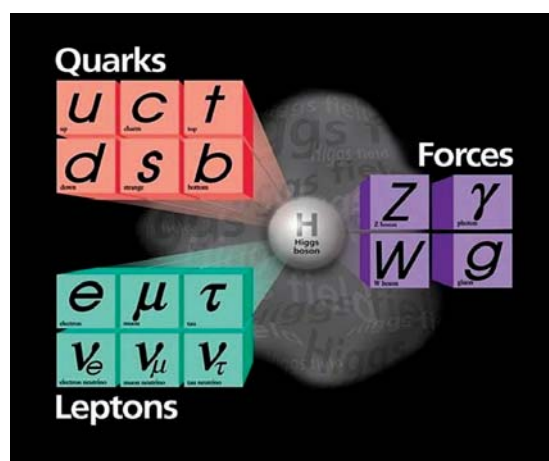
Nuclear physics Division
(for BARC-CMS collaboration)

The European Organization for Nuclear Research (CERN) at Geneva, Switzerland came out with an exciting announcement on 4th July 2012 that two of its major experiments CMS (Compact Muon Solenoid) and ATLAS (A Toroidal LHC Apparatus) had found a new particle which behaves like Higgs boson corresponding to a particle weighing about 125 Giga electron Volts (GeV) and about 133 times heavier than the protons that lie at the heart of every atom. The Higgs particle is the missing piece of the standard model of physics which describes the basic building blocks of the universe, such as protons, electrons and atoms. The Higgs particle is named after Peter Higgs, who was one of six researchers who theorized about the existence of this particle in 1964. It is commonly called the "God Particle", after the title of the book written by Nobel prize winner physicist Leon Lederman "*The God Particle: If the Universe Is the Answer, What Is the Question?*". All elementary particles can be classified either as fermions which follow Fermi-Dirac statistics or bosons which follow Bose-Einstein statistics depending on their intrinsic spin values. The Higgs particle follows the Bose-Einstein statistics and hence, is called a boson which remained elusive for the last 48 years. Finding of the Higgs is vital to the standard model, the theory that describes how elementary particles got their mass and explains the origin of the universe. People all over the world have started congratulating the team of scientists at the Large Hadron Collider (LHC) (which is about 100 meters underground) atom smashing machine covering 27 kms in the Franco-Swiss border. It may be recalled that when LHC machine was about to be operational in 2008, a panic was created in public mind due to the fear that this giant machine is so powerful that it could create a black hole that would

eat up more and more Earth's matter until we and our planet are fully consumed. Contrary to this expectation, nothing unusual has happened today and every one is excited with the news that Higgs like boson has been discovered. A confirmation that this is the Higgs boson would be one of the biggest scientific discoveries of the century. The hunt for the Higgs has been compared by some physicists to the Apollo programme that reached the moon in 1969. In this article, we will briefly discuss (a) What is this God particle-the Higgs boson (b) Why is it important (c) Have we really discovered it and (d) What is the contribution of India in general and BARC in particular to this epoch making Higgs search.

The God particle-the Higgs boson

The Higgs boson or the God particle is the last particle of the standard model whose discovery is yet to be confirmed. The standard model is the name given in the 1970s to a theory of fundamental particles and how they interact. As we know today, the atom contains nucleus comprising of proton



God particle-the Higgs boson

and neutron being surrounded by cloud of electrons. The number of protons and electrons are equal so that the atom as a whole is neutral. For example, a helium atom is made up of a nucleus of two protons, two neutrons (commonly known as alpha particle) being surrounded by two electrons. We also know that each proton carries one unit of positive charge, neutron is neutral while electron is having one unit of negative charge. In 1964, Murray Gell-Mann and George Zweig proposed that nucleons (proton and neutron) are not fundamental as they are made up of sub-structure called quarks which was finally supported by experimental evidence in 1969. The so called standard model emerged incorporating all that was known about subatomic particles at the time and predicted the existence of additional particles as well. There are seventeen named particles in the standard model. It can be divided into three groups: quarks, leptons and force carriers. There are six types of quarks known as up(u), down(d), charm(c), strange(s), top(t) and bottom(b). The up and down quarks are the lighter ones (having mass about few MeV) and the top quark is the heaviest one (mass about 175 GeV) as heavy as a gold atom. The protons and neutrons consist of only up and down quarks. The proton contains two up quarks and one down quark (uud). Each up quark carries a fractional electric charge of $2/3$ while a down quark carries an electric charge of $-1/3$. Similarly, the neutron consists of two down quarks and one up quark (ddu). There are three types of leptons known as electron, muon, tau and their corresponding neutrinos. The quarks and leptons, which in turn are divided into three generations, are members of a family of particles called fermions (particles with half integer spins). Both the quarks and leptons come in pairs. For example, quarks are grouped up-down, charm-strange, and top-bottom. The leptons also come in pairs. The electron, muon and tau particles each have an associated nearly zero mass, charge-less neutrino. The electron is a stable particle and is present in almost all matter. The muon and tau

particles are unstable and are found primarily in decay processes. The intermediate vector bosons or force carriers, make up the third group of the standard model. They transmit three of the four fundamental forces through which matter interacts. The gluon (g) is responsible for the most powerful force, the strong force, which binds quarks together inside protons and neutrons. The photon is the electromagnetic force carrier that governs electron orbits and chemical processes. Lastly, the W and Z bosons are attributed to the weak force, playing a role in radioactive decay. The weak force is very important in observing neutrino reactions. As we know, electron was discovered by J. J. Thompson in 1897. The last particles of the standard model discovered were the W and Z bosons in 1983, the top quark in 1995, the tau neutrino in 2000. Higgs boson is the only missing particle of the standard model until today. The recent reported discovery in 2012 is consistent with this Higgs boson.

Why is it important

The Higgs boson is a fundamental particle of the standard model and is one of the building blocks of the universe. There are other fundamental particles, but this one is special in the sense when the fundamental particles which make up matter interact with the Higgs boson (more specifically with Higgs field), they acquire mass. Higgs also acquires mass interacting with itself. Without this interaction, these particles would have no mass, and would travel at the speed of light, as does the photon. The universe would have been different without mass. For example, if the electron had no mass, there would be no atoms. Hence there would be no ordinary matter as we know it, no chemistry, no biology and no people. The Higgs field fills the universe like water fills a pool. As particles move through the universe they acquire mass by interacting with the Higgs field. One way to imagine the Higgs field is to imagine trying to walk through a pool. The water pushes against you making you feel heavier, and making it harder for you to move. This

effectively generates inertia or mass. Of course, one can climb out of the pool and walk normally. But particles can never escape the Higgs field since it is everywhere, including the vacuum of space. While the above is a simple analogy, the actual Higgs mechanism corresponds to a physical process known as spontaneous symmetry breaking. Let us take an example as to what happens when a magnet is heated above the critical temperature T_c . At high enough temperature, the magnetic property is lost as atomic spins are randomly oriented having zero average magnetization. However, when temperature is lowered below T_c , magnetization is restored as all the atomic spins are aligned in a particular direction having non-zero average magnetization. At high temperature, the average magnetization $\langle\phi\rangle = 0$ and the system is in a symmetric phase where as at low temperature, $\langle\phi\rangle \neq 0$ and symmetry is broken. Similar arguments can be extended to Higgs field as well. All particles had no mass just after the Big-Bang when the universe was created. The average Higgs field or more precisely the vacuum expectation value (vev) of the effective Higgs field was zero. As the universe cooled and the temperature fell below a critical value (about 100 GeV), the vev of Higgs field became non zero. Thus, an invisible force field was formed together with associated Higgs bosons. This is what is called spontaneous symmetry breaking which generates mass for Higgs itself and also generates three massive gauge bosons W^+ , W^- and Z . The fermions like quarks and electrons acquired mass through Yukawa coupling with the vev of the Higgs field. While the W and Z bosons were detected long back experimentally, the associated Higgs boson has escaped detection for the last many years.

Have we really discovered it

On 4th July, 2012 in a joint seminar at CERN, both CMS and ATLAS presented their latest results on the search for the standard model Higgs boson. Both experiments observe a new particle in the mass region around 125-126 GeV. This new particle could be the elusive Higgs boson, which has been

searched for by high energy physicists all over the world for several years.

Due to very short life time (about 10^{-25} sec), Higgs boson, once produced prefers to transform or decay into the heaviest particles it can. The five important decay channels being investigated by CMS and ATLAS experiments are (i) $\gamma\gamma$ channel (gamma-gamma), (ii) ZZ (Z -boson which finally decays to four leptons), (iii) WW (W boson finally decaying to two leptons and two neutrinos), (iv) bb (bottom and anti-bottom quarks) and (v) $\tau\tau$ (tau and anti-tau leptons). Finally, what is being estimated by experiments is the invariant mass M of the decaying particle H which is defined as $M^2 = E^2 - p^2$ where E and p are the energy and momentum of the particle H (in unit of velocity of light). Since H decays immediately into daughter products, in reality, invariant mass of the H particle is estimated from the relation $(E_1 + E_2)^2 - (p_1 + p_2)^2$ where E_i and p_i are the energies and momentum of the decay products.

The CMS team claimed that they had seen a “bump” in their data corresponding to a particle weighing in about 125 GeV. The evidence is strongest in the two-photon final state (gamma-gamma channel) as well as in the final state with two pairs of charged leptons (electrons or muons through ZZ decay). It is interpreted that this could be due to the production of a previously unobserved particle with a mass of around 125 GeV. Within the statistical and systematic uncertainties, results obtained in the various search channels are consistent with the expectations for the standard model Higgs boson. Similar result has also been reported by ATLAS, the other LHC experiment looking for Higgs. Both Higgs decay channels (two photons or four leptons) show statistically significant excess at about the same place. ATLAS reports the mass of the new particle to be 126.0 GeV.

However, more data is needed to establish whether this new particle has all the properties of the standard model Higgs boson or whether some do not match, implying new physics beyond the standard model.

The preliminary results presented will be refined with new LHC data taken this year. These are exciting times for the particle physicist community and the desire to validate the standard model with discovery of Higgs particle is becoming a reality.

Indian contribution: BARC in particular

In this context, it is important to bring out the significant contributions of Indian institutes to the LHC program. We refer to a series of articles published in *Physics News Vol 28, October, 2008* describing in detail the Indian contributions to the LHC programs which we mention briefly in the following sections. Indian institutions took part in two major collaborations at the LHC, CMS and ALICE (A Large Ion Collider Experiment). ALICE is a dedicated experiment to study quark gluon plasma (QGP) that mimics the early universe while CMS is an experiment looking for the Higgs boson as well as QGP formation in heavy ion collision. The CMS experiment consists of groups from BARC (Mumbai), Delhi University (Delhi), IIT (Mumbai), Panjab University (Chandigarh), SINP (Kolkata), TIFR (Mumbai), Viswabharati University (Santiniketan). The ALICE experiment has participation from Aligarh Muslim University (Aligarh), IIT (Mumbai), IOP (Bhubaneswar), Jammu University (Jammu), Panjab University (Chandigarh), Rajasthan University (Jaipur), SINP (Kolkata), VECC (Kolkata). Although the Higgs search using proton beam is one of the primary motivation of CMS experiment, it also records the data when two heavy Lead ions (Pb) collide at relativistic energies. This process creates a soup of quark gluon plasma which mimics the formation of early universe that would have existed a few micro seconds after the big-bang. The BARC group is strongly involved in the study of QGP using CMS detector. Apart from physics interest, Indian groups have contributed significantly in developing software for detector simulations and physics analysis and also have participated in making two major detector components: the outer hadron calorimeter and a part of the preshower detector for the forward electromagnetic calorimeter. The silicon sensors

made for the preshower detector are the first of its kind ever developed in India with active participation by BARC and then given to Indian industries (BEL) for large scale production.

Silicon strip detectors for the Preshower Detector of CMS

BARC supplied about 1500 large area 32-strip silicon strip detectors for the preshower detector of CMS. These detectors are being used as preshower sensors in the electromagnetic calorimeter of CMS for π^0/γ rejection and cover an area of $\sim 40,000$ cm² in the CMS. A specific research and development programme was undertaken by BARC to develop the indigenous technology for these 32-strip silicon detectors. The detectors were fabricated using silicon planar technology which is similar to integrated circuit (IC) technology. Since more than thousand detectors were to be supplied to CERN, the technology development was carried out using the facility of silicon foundry – Bharat Electronics Limited, Bengaluru. Developing silicon detectors with very stringent electrical specifications and uniformity over a large area of ~ 40 cm² was a challenging task. Such technology did not exist in our country. In view of expected radiation damage, the technology development was targeted to produce detectors with high breakdown voltage and low leakage currents for ensuring ten years of operation without failure in the high neutron and gamma radiation environment of LHC.

Resistive Plate Chambers (RPC)

BARC along with Panjab University Chandigarh have also taken part in making Resistive Plate Chamber (RPC), a new type of large area gas detectors which are crucial to signal the passage of a muon through the CMS detector. In the present phase, the experiment runs with three layers of RPCs in the end-caps on either side. It is proposed to install the fourth endcap consisting of RPCs for the CMS muon endcap system during the long shutdown in 2013-2014 in order to improve muon trigger efficiency. Nuclear Physics Division, BARC and Panjab

University, Chandigarh, jointly, have been mandated to built, assemble and characterize 50 RPCs for the upgrade along with Cu cooling systems for the entire 200 chambers being built in collaboration with CERN and University of Ghent, Belgium. NPD has already supplied, ten such chambers to CMS in 2008 and remaining supply is expected to start soon after the arrival of gas-gaps from KODEL, Korea by end of October 2012.

Other Contributions

The RRCAT and BARC have contributed significantly in grid computing and supplying various components of the LHC accelerator. The items that were mass manufactured and delivered included precision motion positioning system (PMPS) jacks, super-conducting corrector magnets, heater discharge power supplies, local protection units etc. In addition to hardware, DAE has also provided expert manpower for several tasks. Team of DAE specialists worked at CERN for around five years and performed complete tests and measurements on full series of magnets. The positive experience with regard to magnet evaluation work, prompted CERN to seek and receive Indian help for commissioning some LHC subsystems. These included cryogenic systems as well as a variety of electronic hardware. As a result of significant Indian contributions to various LHC programs, India is given the observer status at CERN.

Conclusion

The interested reader will find more about the observation of a new boson at a mass of 125 GeV with CMS experiment at LHC in a recent publication in *Physics Letters B*, 717 (2012) 30-61. This is a multi authored land mark publication having 12 authors from BARC. Quoting the conclusion from this paper- *An excess of events is observed above the expected background with a local significance of 5 sigma at a mass near 125 GeV, signaling the production of a new particle which is consistent within uncertainties with expectations for the standard model Higgs boson . The collection of further data will enable a more rigorous test of this conclusion and an investigation of whether the properties of new particle imply physics beyond the standard model.* Similar conclusion has also been drawn by the ATLAS collaboration.

Acknowledgements

We acknowledge the contributions of colleagues from BARC who have been associated with BARC-CMS program at various stages: (listed alphabetically), Chatterjee A, Choudhury R K, Dutta D, Ghodgaonkar M, Jha V, Kailas S, Kumar Vineet, Mishra D, Netrakanti P, Pant L M, Shukla P, Topkar A. We also pay special tribute to late Dr. S. K. Kataria who was the first person to initiate the BARC-CMS collaboration with CERN.

Bioremediation: Discovery of a Novel Alkaline Phosphatase through X-Ray Crystallography

Subhash C. Bihani, Shree Kumar Apte, Jean-Luc Ferrer and Madhusoodan V. Hosur*

Solid State Physics Division and Molecular Biology Division

Abstract

Alkaline phosphatase (AP) is a bi-metalloenzyme with potential applications in biotechnology and bioremediation. The enzyme hydrolyses nonspecifically phosphate monoesters under alkaline conditions to yield inorganic phosphate. The AP isolated from the bacterium *Sphingomonas sp.* Strain BSAR-1 (SPAP) was shown to be particularly useful for the recovery of uranium from alkaline radioactive waste. We report here the first X-ray crystal structure of SPAP determined by using the Multi-wavelength Anomalous Diffraction method to solve the phase problem. The crystal structure shows that the enzyme active site is similar to those in other APs with two Zn^{2+} ions in the core, even when there is a large difference in the rest of the tertiary structure. Structural differences observed are: 1) threonine as the catalytic residue instead of serine, 2) absence of third metal ion binding pocket, 3) deletion of the arginine residue forming bidentate hydrogen bonding with the substrate phosphoryl group, and 4) recruitment into the active site of lysine171 and asparagine110 residues to bind the substrate phosphoryl group in a manner not observed before in any other AP. These structural differences suggest that SPAP represents a new class of APs and also provides important insights into evolutionary relationships between members of AP superfamily. Because of its direct contact with the substrate phosphoryl group, lysine171 is proposed to play a significant role in catalysis.

Introduction

(a) Bioremediation

Nuclear materials are being used for a variety of purposes ranging from electrical power generation, to nuclear weapons development to disease diagnosis and treatment. Various steps in the nuclear fuel cycle generate, as intermediates, large amounts of radioactive materials [1]. Environmental contamination due to release of radionuclides during storage is a major worry for the nuclear industry. According to U.S. Environmental Protection Agency (EPA), over 1,000 United States locations are contaminated with highly energetic radionuclides including ^{235}U [2]. Currently available chemical methods for cleanup are costly and often lack the specificity required to properly decontaminate. Bioremediation of heavy metal contamination using radiation-resistant microbes provides an effective and more economical alternative. Microbial precipitation of uranium in the form of uranyl phosphate also allows recovery of precious metal from very low concentrations [3]. Recently, Kayzad et al. [4] have

cloned into *Escherichia coli*, the alkaline phosphatase from *Sphingomonas sp.* strain BSAR-1, labeled here as SPAP, and the recombinant *E. coli* strain over-expressing SPAP was found to be very efficient in bioprecipitation of uranium as uranyl phosphate. SPAP exhibits several unique features, such as constitutive expression, thermo-lability, extracellular release and high specific activity [5], which make SPAP an ideal reagent also for many biotechnological applications. Atomic-level structure in three dimensions, that can be determined using crystallography, would provide critical input for further improving the utility of SPAP in bioremediation and biotechnology [6].

(b) The Crystallographic method

The basic principle of the crystallographic method is the Fourier relationship between scattering density distribution $\rho(xyz)$ and its diffraction pattern $\mathbf{F}(hkl)$. When the sample is in the form of a single crystal of the molecule under study, the Fourier transform is sampled at discrete points determined by the unit cell parameters. Then the Fourier relationship can be written as a series summation given below:

*Corresponding author

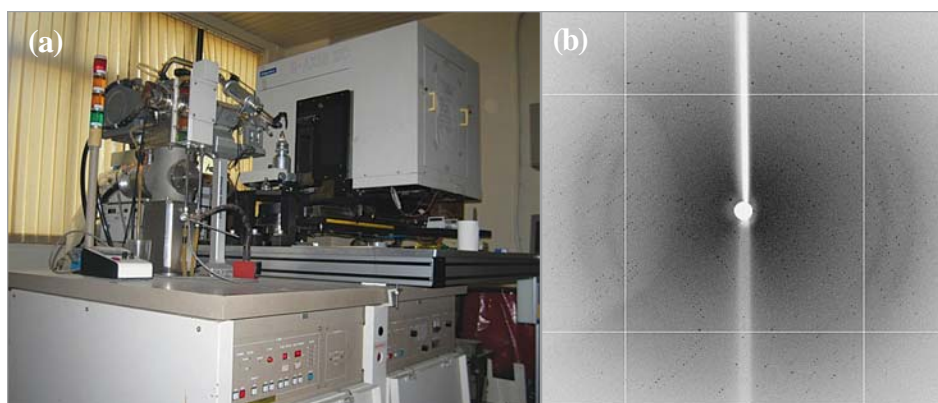


Fig. 1: a) RAXIS -IIC single crystal IP X-ray diffractometer. b) typical oscillation diffraction photograph from SPAP crystal.

$$\rho(xyz) = \frac{1}{V} \sum_{hkl} |F_{hkl}| \exp(i\alpha_{hkl}) \exp[-2\pi i(hx + ky + lz)]$$

where h , k , and l are integers that specify spatial direction of the Bragg reflection (hkl), and $F(hkl)$ is the complex structure factor characterized both by a magnitude, $|F(hkl)|$, and a phase, $\alpha(hkl)$. The set of values of the function $\rho(x,y,z)$ at different (x,y,z) positions constitutes the electron density map, which represents the three dimensional structure of the molecule. All atoms in the molecule will lie inside the cage defined by positive contours in the electron density map. However, in a diffraction experiment, only the magnitudes of the structure factors are derived from the measured intensities, and separate strategies have to be used to obtain the phases before Fourier summation can be carried out. Although there are many different methods for actual recording of Bragg reflection intensities, the fastest one is the oscillation method, which uses a single-axis goniometer and a stationary two-dimensional X-ray detector positioned perpendicular to the monochromatic X-ray beam incident on the crystal, as shown in Fig. 1a. The crystal is oscillated about an axis perpendicular to the X-ray beam direction, and the diffracted rays emanating in different directions are intercepted on the detector. The total diffraction data is measured as a series of non-overlapping oscillation frames recorded about contiguous positions of the crystal, and all these frames together constitute one data set. A typical oscillation diffraction photograph is shown in

fig. 1b. Each dark spot visible in Fig. 1b is a Bragg reflection, whose characteristic indices (h,k,l) and intensity I_{hkl} are established during 'processing' of the oscillation frame.

The oscillation angle and the total number of frames to be recorded depend on the crystal symmetry, unit cell parameters, and the redundancy required. As already mentioned above, in a diffraction experiment, one obtains only the magnitude of the structure factor. Not knowing the phases of reflections is described as the 'phase problem' in crystallography, and a variety of methods to obtain reflection phase have been developed over the last century. One of the more recently developed methods is the Multi-wavelength Anomalous Diffraction method (MAD) [7, 8]. This method exploits the physical fact that atomic X-ray form factors become complex and change rapidly with wave length near the atomic absorption edges. The exact atomic absorption edge is sensitive to the environment within the crystal, and therefore, has to be derived by using *in-situ* X-ray absorption/fluorescence measurements. In a MAD experiment, the wave lengths used for data collection differ in energy by only a few electron volts, and therefore synchrotron beamlines with energy resolution of the order of 10000 are required. Further, since the anomalous differences are rather small, the reflection intensities have to be measured very accurately. The

phases derived using MAD method are generally superior compared to other methods, and lead to cleaner and easily interpretable electron density maps. The structure of SPAP is one of the first structures to be determined in India using the MAD method.

(c) Alkaline phosphatase

Alkaline phosphatases (APs) are enzymes that hydrolyze phosphate monoesters under alkaline conditions to yield an alcohol and inorganic phosphate. APs are metallo-enzymes, and crystal structures show that their active sites contain the bi-metallo-zinc core and a Mg^{2+} ion, which are involved in a two stage catalytic mechanism [9, 10]. Multiple sequence alignment shows that there is very little similarity in the amino acid sequences of SPAP and other APs. Interestingly, SPAP has highest sequence similarity with nucleotide pyrophosphatases (NPP), but does not have pyrophosphatase activity. The three dimensional structure shows that SPAP is a unique alkaline phosphatase representing a new class.

Experimental

Overexpression, Purification and Crystallization of SPAP protein

Gene for SPAP protein was cloned and protein was over-expressed in *E.coli* as described [4]. Crystallization was performed at 298 K by sitting-drop vapor diffusion method in 96-well crystallization plates (Greiner, 3cup) using Cy-Bio HTPC robot [5, 6]. Both native as well as Seleno-MET(SM-SPAP) crystallized under several conditions. Crystallization condition for SM-SPAP was optimized manually by hanging-drop vapor diffusion method [6].

X-ray Diffraction Data collection & Structure Determination

X-ray diffraction data for both native and SM-SPAP crystals were collected at 100 K by using the oscillation method and the FIP beamline on the European Synchrotron Radiation Facility (ESRF). A fluorescence scan on SM-SPAP crystals enabled

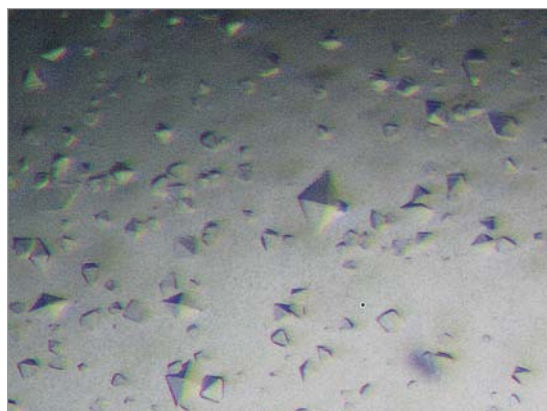


Fig.2: Single crystals of SPAP grown by vapour diffusion. The largest dimension of the biggest crystal is about 0.1 mm. The crystals are well ordered and diffract X-rays to high resolution. Crystals of SM-SPAP also were similar in shape and size. Both SPAP and SM-SPAP crystals belong to the space group $P4_12_12$.

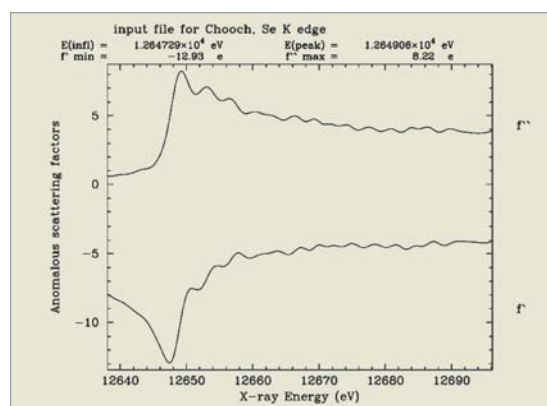


Fig. 3: Anomalous scattering factors for selenium atoms in the crystal derived from the X-ray fluorescence spectrum recorded on the crystals. Energies corresponding to anomalous peak and inflection points are listed.

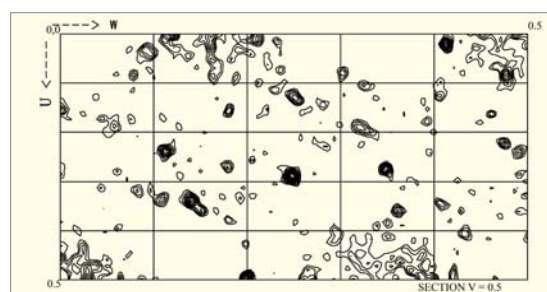


Fig. 4: The $V=0.5$ Harker section of anomalous difference Patterson map showing good quality of the measured anomalous signal. The maps are contoured at intervals of 0.5σ , starting from 1.0σ . Interpretation of the four Harker sections of the space group yielded 12 Selenium sites.

identification of the three wavelengths for a MAD data collection. At each wavelength, 180 diffraction images, each for an oscillation angle of 1° and an exposure time of 60 seconds, were recorded. For native crystals 180 diffraction images at a single wave length were recorded, again for an oscillation angle of 1° and an exposure time of 60 seconds. Experimental phase determination and initial molecular model building were carried out using the AutoSol and AutoBuild tools in the software suite PHENIX [11]. The fit of the atomic model to the experimental electron density was improved manually by using software package Coot [12]. The software phenix-refine was used to execute standard protocols of simulated annealing (SA) and TLS refinement [13]. The native structure was later solved by using the protein part of SM-SPAP structure as a search model in Molecular Replacement calculations [11]. The procedures used for refinement of the native structure were same as described above.

Results and Discussion

The tetragonal crystals of SPAP are shown in Figure 2. Crystals of SM-SPAP also have similar morphology, and both belong to the space group $P4_12_12$, and contain one SPAP monomer

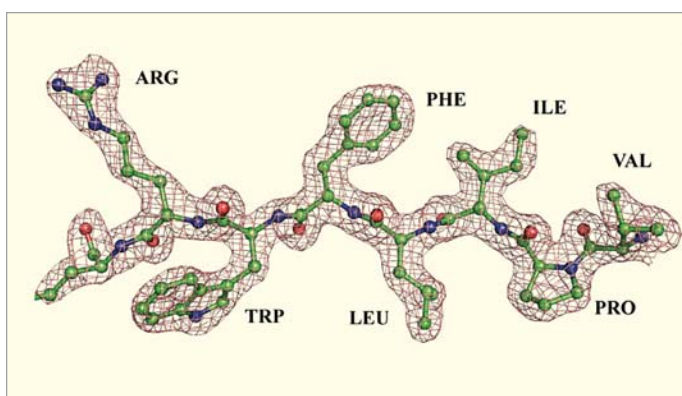


Fig. 5: A region of the electron density map overlaid with the corresponding backbone and side chain atoms of a seven residue segment in SPAP. Atoms are drawn as coloured spheres (carbon –green, nitrogen – blue and oxygen – red), and interatomic bonds are drawn as sticks. Note that the atomic model is completely inside the electron density cage. The amino acid sequence of this protein-segment is VAL-PRO-ILE-LEU-PHE-TRP-ARG in three letter code. The entire map is of similar quality.

(559 residues) per asymmetric unit. High resolution diffraction data from both SPAP and SM-SPAP crystals were collected using the FIP beamline on ESRF at Grenoble, France. Crystal parameters and data collection statistics are given in Table 1. The crystal structure was solved by using the MAD method to determine reflection phases. The wavelengths for MAD data collection were determined by analysing the X-ray fluorescence spectrum (Fig. 3, Table 1).

Fig. 4 is one of the four Harker sections of the anomalous difference Patterson map showing good quality of measured anomalous signal that led to Se-atom substructure. Refinement statistics for the anomalous scatterers are given in Table 1. Fig. 5 shows the experimentally obtained electron density cage contoured at 1.5σ level for a short segment of the protein chain. It is clear that all atoms of the atomic model are very well contained within the electron density cage, highlighting the accuracy of the derived structure. The accuracy of the structure is also evident from the low crystallographic R-factors (Table 2), which are a measure of the agreement between observed and model-derived intensities of Bragg reflections. The final contents of the asymmetric unit are: 526 protein residues (31–556) comprising of 4022 non-hydrogen atoms, two zinc ions of partial occupancy (0.75), 278 water molecules,

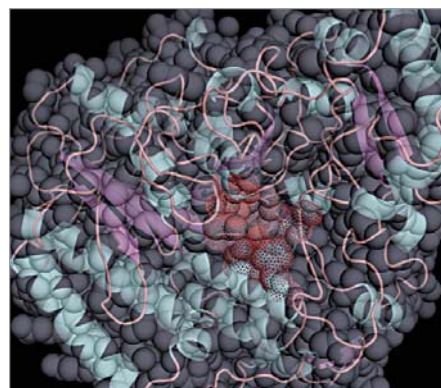


Fig. 6: Space filling model overlaid with the cartoon showing β -strand (magenta) and α -helical (cyan) regions of SPAP. The active site residues in the middle of the figure are coloured brick red.

5 glycerol molecules, 1 Ca^{2+} ion and one molecule of an organic phosphate in the active site. The protein model has good stereochemistry with 98% residues lying in the most favoured region of Ramachandran map.

Molecular Conformation

The overall shape of the polymeric protein chain is shown by a space filling diagram in which each atom is drawn as a sphere of radius proportional to the van der Waal radius of the atom (Fig. 6). Segments of the protein backbone fold into α -helices and β -strands, which are shown in fig. 6 as a cartoon overlaid on the space filling diagram. These secondary structure elements then associate to give the protein a specific three dimensional shape. The shape can be described as that of a shallow cup with a thick base. The protein has two domains, one large N-terminal domain forming the base and most of the wall region of the cup, and a smaller C-terminal domain (right extreme portion in Fig. 6) forming the handle. N-terminal domain consists of an eight-stranded mixed central beta sheet (shown in magenta) surrounded by α -helices (shown in cyan) while the smaller C-terminal domain primarily consists of a single two-stranded antiparallel beta

hairpin covered by two α -helices on the surface. The physical size of the protein molecule can be estimated by noting that the alpha helix has a pitch of 5.4 Å. The active site (shown in brick red), located at the bottom of the wide and shallow opening of the cup is exposed to the environment.

Active Site

Active site of SPAP is geometrically identical to that in ECAP, and contains two metal ions (M1 and M2), which were identified as Zn^{2+} through X-ray fluorescence measurements. Distance between the two metal ions is 4.1 Å. M1 coordinates directly to the hydroxyl group of Thr89, confirming Thr89 to be the catalytic residue in SPAP, as suggested by sequence alignment. The other amino acid residues coordinated by the zinc ions are identical to those in ECAP.

Polar Lysine residue replacing the third metal

The third metal ion, mostly Mg^{2+} , invoked in the catalytic mechanism is bound at a site shown to be conserved in crystal structures of ECAP-like APs. However, in SPAP, there is no such third metal ion coordination site because, structural superposition shows that non-polar amino acids Ala174 and

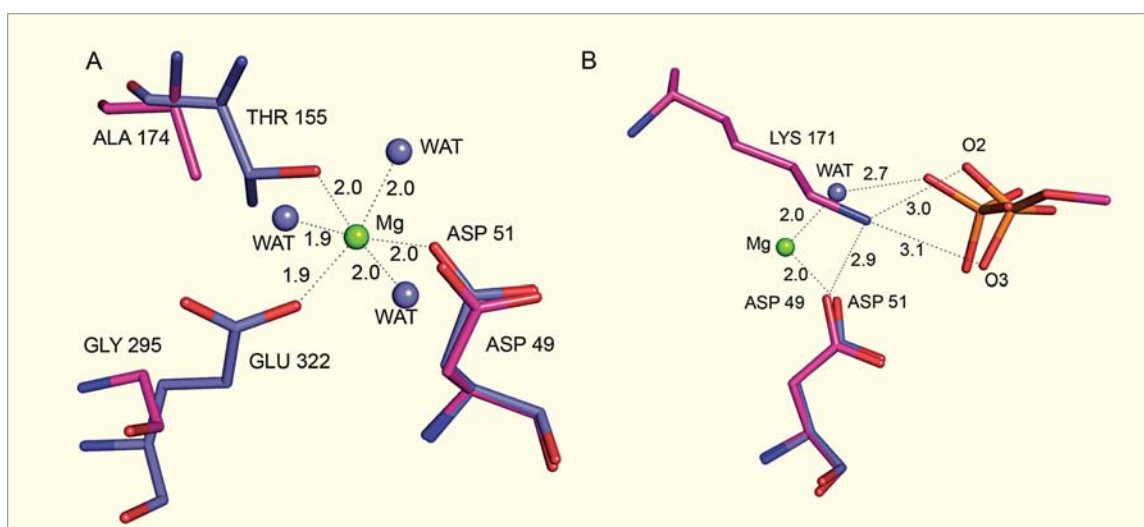


Fig. 7: Structural superposition of SPAP (magenta) and ECAP (blue) around the Mg^{2+} -binding site in ECAP. (A) Abolition of Mg^{2+} ion binding site. Polar residues coordinating Mg^{2+} ion in ECAP are missing in SPAP. (B) Introduction of Lysine in the active site of SPAP. Lys171 in SPAP interacts with the substrate in a way analogous to Mg^{2+} ion in ECAP.

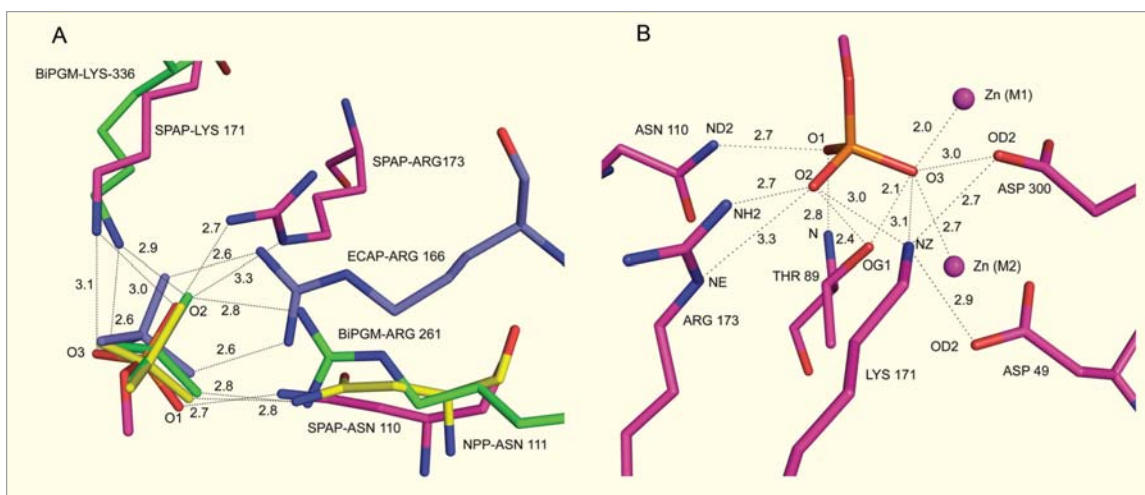


Fig. 8: Comparison of interactions between substrate phosphoryl group and the amino acid residues in the active site: (A) NPP – yellow, BiPGM - green, ECAP – blue, and SPAP – magenta; (B) zinc ions in the active site of SPAP. Hydrogen bond distances are also indicated.

Gly295 now occupy positions of amino acids Thr155 and Glu322 that coordinate Mg^{2+} ion in ECAP (Fig. 7A). Interestingly, the structure reveals that a lysine residue, which has a positively charged N atom at the end of the side chain, is positioned exclusively in the active site of SPAP. This N atom is involved in chemical interactions similar to those of Mg^{2+} in ECAP-like enzymes (Fig. 7B). These observations suggest that Lys171 in SPAP is substituting for Mg^{2+} ion in ECAP.

SPAP – A novel AP representing a New Class

There are several features which make SPAP a novel AP. First, the key catalytic residue in SPAP is Thr89 instead of serine found in all other APs. Second, the conserved third metal ion binding pocket in the active site in ECAP-like APs, is absent in SPAP (Fig. 7A and 7B). Third, the active site arginine residue conserved in ECAP-like APs is absent in SPAP (Fig. 8A and 9). Fourth, the sequence identity between SPAP and ECAP-like APs ranges from 12% to 14.6%, which is very low compared to the range of 30% - 50% observed among ECAP-like APs (Fig. 9). Fifth, the combined presence in the SPAP active site of key amino acid residues Thr89, Asn110, Lys171 and Arg173 (Fig. 8B and 9), observed only separately in the active sites of members of the AP superfamily. Interestingly, the relative positions and interactions

of these residues with the substrate phosphoryl group are maintained in the individual active sites (Fig. 8A).

Implications toward Molecular Evolution

Proteins with related functions and similar structure are combined into a larger group called as a superfamily. APs are part of a superfamily, which includes nucleotide pyro-phosphatases (NPP), co-factor independent phosphoglycerate mutases (iPGM), phosphonate monoester hydrolases (PMH) and aryl sulfatases (AS) [14]. Amino acid sequence similarity between different members of the superfamily is often too low to reveal relatedness. In such conditions, structural alignment method can provide better understanding of molecular evolution. Structural alignment, using the DALI server [15], shows that SPAP has highest similarity with NPP (Z-score 28.2) rather than with ECAP (Z-score 20.1) or other ECAP like APs. Structural superposition also shows that the substrate-interaction pattern observed in SPAP is different from that seen in ECAP and other APs. The two coplanar hydrogen bonds to the substrate phosphoryl group from the conserved active site arginine residue in all ECAP-like APs are absent in SPAP. Instead, there are two non-coplanar hydrogen bonds to the substrate phosphoryl group from two separate amino acids in the active site

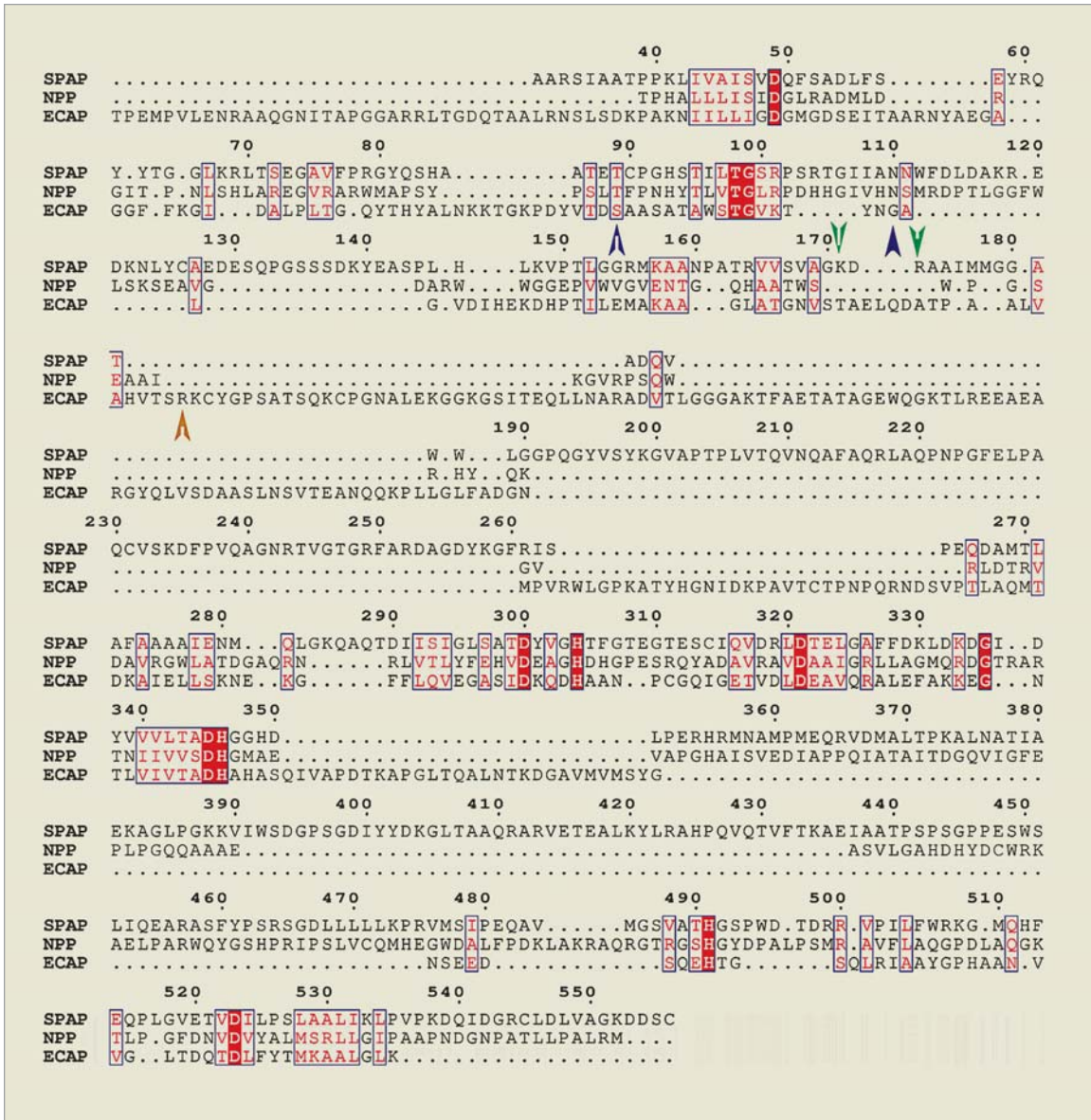


Fig. 9: Sequence alignment derived from structural superposition of SPAP, ECAP and NPP. The amino acid residues are described in single-letter-code. Absolutely conserved residues are shown in red background. Following four novel features of SPAP are highlighted by arrows: 1) presence of Thr89 in place of catalytic serine- blue arrow, 2) presence of unique Lys 171 and Arg173-green arrows, 3) presence of Asn110-blue filled arrow and 4) deletion, in SPAP, of conserved arginine – yellow arrow.

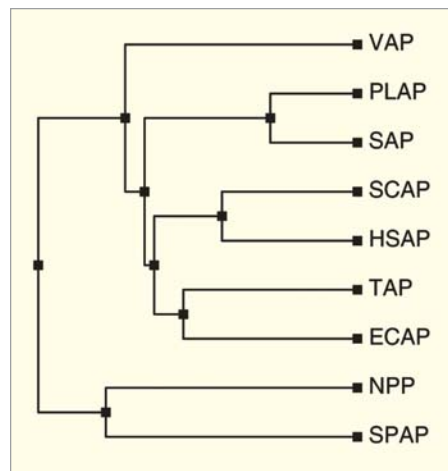


Fig. 10: Phylogenetic tree for alkaline phosphatases.

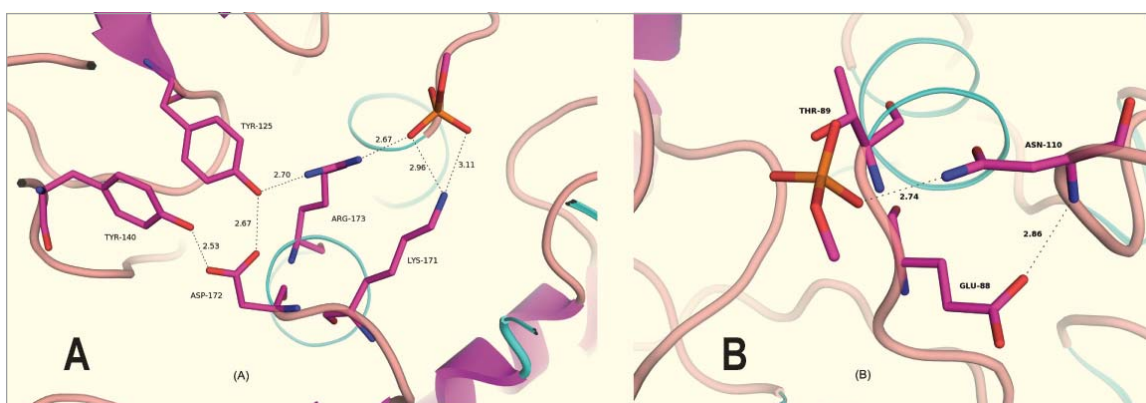


Fig. 11: Hydrogen bonding interactions, near the active site, which may be modulated to increase flexibility of ARG-173 and ASN-110: (A) positioning of ARG-173 and (B) positioning of ASN-110.

Engineering SPAP for higher activity

The alkaline phosphatase enzyme is widely used in the fields of molecular biology and biotechnology.

In fact there are three commercial preparations of APs from different sources, and none of these has totally satisfactory properties of thermolability and

Table 1: Crystal data, intensity data and anomalous phasing statistics for SM-SPAP.

	MAD dataset		
	peak	inflection	remote
Unit Cell (Å)	a = 87.20 b = 87.20 c = 165.2		
Wavelength (Å)	0.980159	0.980337	0.976261
Upper Resolution limit (Å)	1.85 (1.9-1.85)*	1.85 (1.9-1.85)	1.9 (2.0-1.9)
Space group	P4 ₁ 2 ₁ 2	P4 ₁ 2 ₁ 2	P4 ₁ 2 ₁ 2
Number of measured reflections	771391 (56396)	771426 (56386)	713097 (92791)
Completeness (%)	100 (100)	100 (100)	99.3 (95.4)
Multiplicity	7.44 (7.08)	7.42 (7.05)	7.47 (7.11)
R-sym (%)	7.3 (49.8)	7.0 (53.8)	8.0 (56.7)
Average I/σ(I)	20.2 (4.13)	20.9 (3.82)	20.3 (3.89)
Anomalous Phasing			
Refined f' (e-)	-7.1	-9.5	-2.1
Refined f'' (e-)	10.6	6.6	6.2
Mean figure of merit	0.58		

*The numbers between parentheses indicate the value in the outer resolution shell

Table 2: Diffraction data and refinement statistics for native SPAP.

Unit Cell (Å) and space group	a = b= 87.37, c = 168.16 , P4 ₁ 2 ₁ 2
Resolution limits (Å)	50 - 1.95 (2.05-1.95)*
Number of reflections measured	379964 (44099)
Average I/σ(I)	13.02 (2.15)
R (%)	15.53
R _{free} (%)	18.63
No. of protein atoms	4022

*The numbers between parentheses indicate the value in the outer resolution shell. R.m.s= root mean square.

high activity. Therefore, there is a demand for an AP which has high activity, can be purified in large amounts, and can be easily and completely inactivated by heating to milder temperatures. SPAP has favourable properties in these respects. Since greater flexibility in and around the active site is correlated with higher activity, we have identified Glu88, Tyr125 and Asp172 as residues that can be mutated to impart flexibility to the active site residues Arg173 and Asn110, which are binding the phosphoryl moiety (Fig. 11A and 11B).

Acknowledgments

This work was carried out as part of an MOU between BARC, India and CEA, France, for cooperation in the field of life sciences. MVH is thankful to Drs. R. Chidambaram and K. K. Kannan for scientific discussions. We are thankful to the National Facility for Macromolecular Crystallography, SSPD, BARC for providing access to the equipment.

References

- Lloyd J R and Renshaw J C (2005) *Curr Opin Biotech* 16:254–260.
- <http://www.epa.gov/radtown/clean-up.html>.
- Basnakova G, Stephens E R, Thaller M C, Rossolini G M and Macaskie L E (1998) *Appl Microbiol Biotechnol* 50:266–272.
- Nilgiriwala K S, Alahari A, Rao A S, Apte S K (2008) *Appl Environ Microbiol* 74: 5516-5523.
- Nilgiriwala K S, Bihani S C, Das A, Prashar V, Kumar M, et al. (2009) *Acta Cryst F65*: 917-919.
- Bihani S C, Das A, Nilgiriwala K S, Prashar V, Pirocchi M et al (2011) *PLoS One* 6: e22767.
- Ramaseshan S and Abrahams S C (1975) *Acta Cryst B24*, 35 – 39.
- Sikka S K (1969) *Acta Cryst A25*: 396-397.
- Kim E E, Wyckoff H W (1991) *J Mol Biol* 218: 449-464.
- Stec B, Holtz K M, Kantrowitz E R (2000) *J Mol Biol* 299: 1303-1311.
- Adams P D, Afonine P V, Bunkoczi G, Chen V B, Davis I W, et al. (2010) *Acta Cryst D66*: 213-221.
- Emsley P, Cowtan K (2004) *Acta Cryst D58*: 2126-2132.
- Painter J, Merritt E A (2006) *J Appl Cryst* 19: 109-111.
- Galperin M Y, Bairoch A, Koonin E V (1998) *Protein Sci* 7: 1829-1835.
- Holm L, Rosenström P (2010) *Nucleic Acids Res* 38: 545-549.

Improved Location of Earthquakes in Sumatra Region using Gauribidanur Seismic Array Data

Manoj Kumar and Falguni Roy
Seismology Division

Abstract

The aim of this study has been to explore the applicability of an event location method based on PcP and various depth phases, particularly for the earthquakes in Sumatra region with a reasonable degree of accuracy using Gauribidanur short period seismic array data. The method utilizes PcP–P time based distance estimate along with depth and azimuth of the source for locating events in this region. The task to identify PcP and depth phases is accomplished using array beaming technique that facilitates identification of these phases by virtue of their slownesses across the array. Slowness measurements have been carried out using a software package named SPIDER (Seismic Phase Identifier for Depth and Epicenter Reassessment), developed in Seismology Division, BARC. It has been demonstrated that the arrival time information of PcP and various depth phases obtained from the analyzed array seismogram, together with source azimuth, can be successfully used to reliably locate earthquakes of magnitude ≥ 5.5 in Sumatra region.

Introduction

Seismic arrays play a significant role when it comes to enhancement of weak signals, estimation of apparent velocities of various seismic phases and determination of azimuth to an event. Enhancement of weak signals is achieved through a method known as beam-forming. If the ambient noise is completely incoherent and the signal is fully coherent across the array, beam-forming or delay and sum processing of the array data from N sensors would provide a signal to noise gain of \sqrt{N} as compared to a single seismometer. In view of this seismic arrays have the potential to facilitate detection of weak signals. Subsequent to detection of a signal, the next important task, perhaps, is to find the location of the source that generated the signal. In order to locate an event from one point on the earth, e.g. a seismic array, to another point where a seismic event has taken place, we need to know the distance and azimuth from the array to the source epicenter. The azimuth to an event can be estimated at a two dimensional seismic array from the observed signal time delays across the array. The distance can be estimated either from the arrival time difference between P wave and other later phases such as S,

Lg or PcP waves or from the apparent velocity (V_a) of the P wave which is the inverse of the derivative of travel time with respect to epicentral distance, Δ . The accuracy of this method, however, depends on the slope of $dT/d\Delta$ versus Δ curve. Besides this, knowledge of regional and local travel time variations also plays a significant role in accurate distance estimation (Dahlman and Israelson, 1977). In view of these limitations, former method of distance estimation based on time differences of P and some later phases such as S, Lg or PcP are of more practical value. However, Lg waves are not observed after approximately 100 km of propagation in the oceanic crust, due to which they are not useful for locating undersea earthquakes.

Figure 1 shows various seismic body wave phases comprising depth phases and other surface reflections used in the study.

PcP–P time can provide source distance with reasonable accuracy for distances upto ~ 5000 km which will be comparable to S–P time based estimates provided S phase onset is picked up accurately. However, S onsets upto a distance of

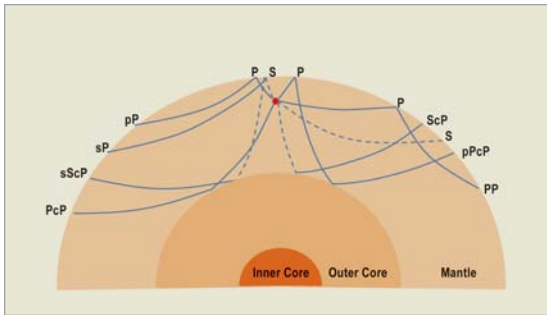


Fig. 1: Various seismic body wave phases comprising depth phases and other surface reflections used in the study. Small red circle indicates the seismic source. Continuous lines show P rays whereas broken lines show S rays. PcP and ScP stands for P and S phases getting reflected at the outer core respectively and further travelling as P waves.

~ 25 degrees is not satisfactorily readable in normal earthquakes, but is very clear in deep ones (Jeffreys and Bullen, 1958). On the other hand, though, PcP may not be detected for small earthquakes, for moderate to large magnitude earthquakes PcP phase can be identified unambiguously based on its slowness across an array and thereby onset of the phase can be accurately picked using data from the seismic array. Further, PcP- P time is less sensitive to depth variation than S-P time.

In the present work, we have set our objective to locate moderate to large magnitude earthquakes in Sumatra region with reasonable accuracy using Gauribidanur seismic array (GBA) data alone. In view of this, we have explored the applicability of PcP-P based distance estimation method together with azimuth of the source for locating events in this region. Attempt has also been made to estimate source depth using depth phases by identifying them based on their slownesses across the array. In general, better estimates of source depth as well as epicentral location of an event may be obtained using a network of seismic stations in comparison to a seismic array, however as mentioned earlier, our aim in this study has been to locate undersea earthquakes in Sumatra region using GBA data, primarily, by exploiting the potential of the array to facilitate identification of PcP and depth phases through the measurement of their slownesses.

The Method of Phase Identification

At the core-mantle boundary, which is having a sharp velocity discontinuity, body waves can undergo reflection as well as refraction. The reflected P waves are called PcP (see Fig. 1). The PcP signal as observed at a seismic array will always have larger apparent velocity as compared to the P signal from the same event. Since both these signals arrive from a fixed direction, the PcP phase can be easily identified from its apparent velocity, which is estimated by forming a large number of beams with different apparent velocities, keeping station to source azimuth constant, and choosing the one that is consistent with the apparent velocity of the P phase. Azimuth, however, can be estimated from the observed P wave time delays across the two arms of the array. Having identified the PcP signal, the difference in travel times between PcP and the P phase can be gainfully employed to estimate the epicentral distance of the event with respect to the array cross over point. This is primarily due to the fact that PcP - P time increases rapidly as the epicentral distance (Δ) reduces, especially for distances below 50° (see Fig. 2). However, S-P time may be used to estimate epicentral distance reliably even for larger distances provided the source depth is known.

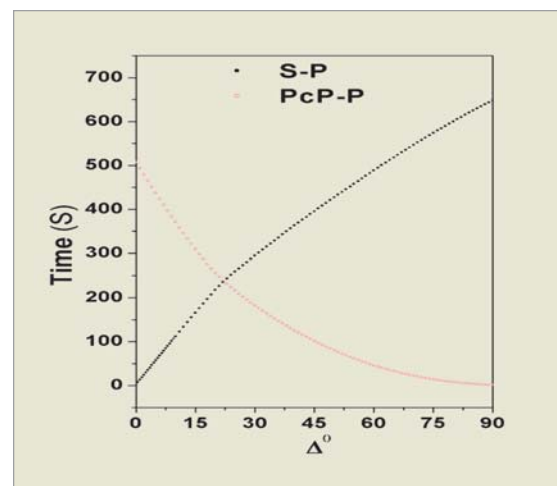


Fig. 2. Variation in PcP- P and S-P times with epicentral distance for surface focus events

Depth phases, viz. pP and sP, that arrive at the receiver as P waves are better identified using a network of seismic stations with varying source station distances (Roy, 1984). However, on short period vertical component seismograms, sub oceanic earthquakes, such as most earthquakes in Sumatra region, can give rise to water surface reflections (pwP and swP) with amplitudes comparable to pP and sP phases (Mendiguren, 1971; Forsyth, 1982; Engdahl and Billington, 1986). Thus, while analyzing seismograms generated by sub oceanic events, care has to be taken that water surface reflections are not identified as pP phase. For unambiguous estimation of source depth using the data from a short period seismic array only, it is necessary that the depth phases pP and sP which may occasionally be obscured by the P coda are further identified with the help of pPcP, sPcP or sScP phases if observed in the seismogram. The phases pPcP and sScP, if observed, can help to distinguish pP phase from pwP phase. Various depth phases can be identified by their apparent velocities. For example, pP and sP will have apparent velocity comparable to P phase whereas pPcP and sPcP will have apparent velocity comparable to PcP phase. Likewise sScP will have apparent velocity comparable to ScP phase.

Phase Identification Software

Software named SPIDER (Seismic Phase Identifier for Depth and Epicenter Reassessment) has been developed at Seismology Division, BARC, using Microsoft Visual Basic (6.0). This software helps user to detect and identify various seismic phases using Gauribidanur array data. It essentially works on the array beaming technique and facilitates identification of phases by virtue of their slownesses across the array. The case studies that follow have been generated using this software.

Case Studies

In order to demonstrate the efficacy of PcP, ScP and various depth phases in locating a seismic event we have presented here the analysis of GBA seismograms pertaining to four events which

occurred in Sumatra region. The digital short period data at GBA are sampled at a rate of 40 samples/s for each of the 20 sensors. A schematic diagram of the array is shown in Fig. 3. Various system details and design characteristics of GBA are available elsewhere (Birtill and Whiteway, 1965; Mowat, and Burch, 1974; Roy and Nair, 2005). A comparison between estimated locations and the locations reported by the United States Geological Survey (USGS) for the analyzed events is presented in Table I.

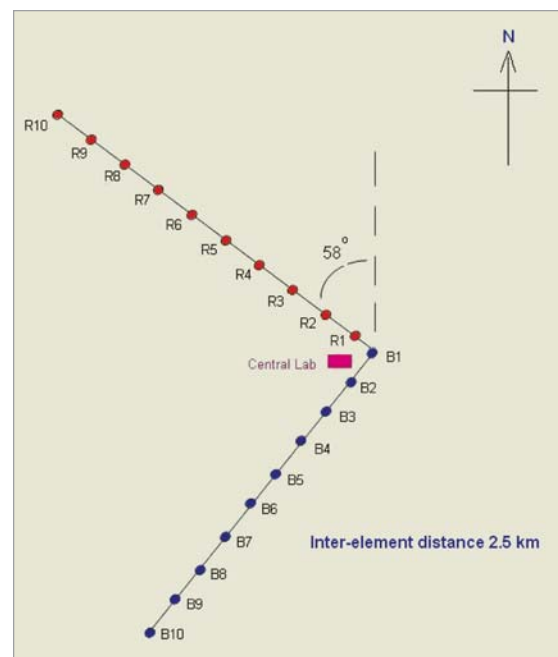


Fig. 3: Layout of the Gauribidanur seismic array. Two perpendicular arms, each comprising ten sensors, are named as Red(R) and Blue (B) respectively.

Event 1

Fig. 4 shows the 20 channel seismogram of event-1 that occurred in Southern Sumatra region. Beginning with the P phase, the seismogram depicts a number of later phases. Detailed analysis to identify these phases is presented in Figs. 5 and 6.

Keeping azimuth fixed at 118.5° , which was estimated from P wave move out across the array, time average products (TAP; Weichert, 1975) were computed using two beams corresponding to RED and BLUE arm channels of GBA for each V_a from 7 km/s to 55 km/s (indicated at the extreme left of

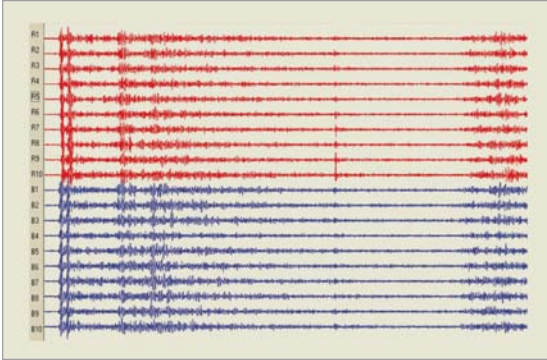


Fig. 4: Short period seismograms at Gauribidanur array corresponding to an earthquake (event-1, table I) in Southern Sumatra region. Plot duration is 360 s. Sensor names are shown at the left.

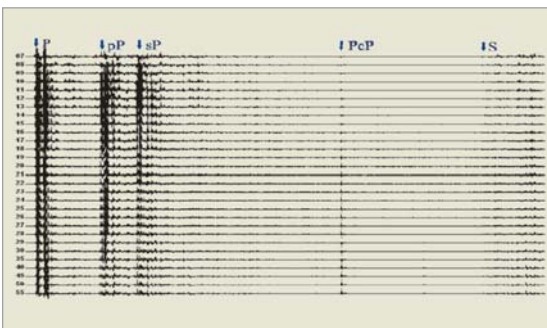


Fig. 5: TAP signals for various apparent velocities (indicated at the left) and fixed azimuth, 118.5° , obtained from P wave move out pertaining to event-1. Duration of the plot is 350s.

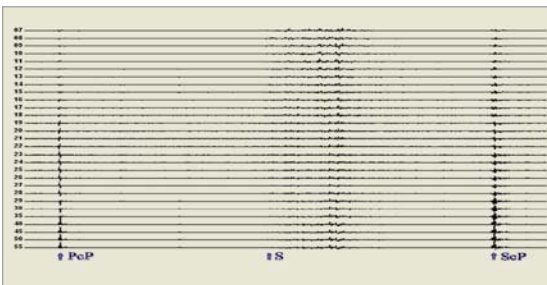


Fig. 6: TAP signals of PcP and ScP phases for Event-1. Duration of the plot is 240s.

the Fig.s 5 and 6). The depth phases pP and sP showed high amplitudes on TAP waveforms at those values of V_a which were close to that of the P wave (see Fig. 5). As the V_a deviated from these values, the amplitudes of the depth phases showed marked reduction. Since the depth phases follow more or less the same path as that of P phase, the values of V_a of these phases are also very similar to that of the P phase. However, as the PcP phase arrives with

a larger value of V_a than that of P wave, the amplitude of this phase slowly builds up in the beamed signal as V_a is increased beyond that of P or depth phases, and starts reducing after attaining the optimum value (see Fig.s 5 and 6). Like PcP, ScP phase also arrives with a larger V_a as compared to P phase. Thus ScP phase can be identified from its V_a (see Fig. 6). Having identified PcP or ScP phase, the distance to the source is obtained from PcP – P time or ScP-P time, which along with source azimuth and depth (obtained from depth phases) may be used to obtain the source location. Table 1 shows the estimated parameters for event-1 as obtained using SPIDER

Event 2

Fig. 7 shows the TAP signals for various values of V_a corresponding to event-2 for constant event azimuth. For this event several phases appeared with the apparent velocity close to that of P wave. Identification of depth phases was difficult from these signals alone. However, when the seismograms were beamed for V_a close to that of ScP phase (approximate time of the ScP phase was available from V_a of P wave), prominent ScP and sScP phases were observed (see Fig. 8). Based on sScP-ScP time, it was possible to identify pP phase unambiguously as indicated in Fig. 7. The event was relocated using ScP – P time and azimuth to the event. PP phase, with low V_a value, was identified based on the epicentral distance of the event.

Event 3

Fig. 9 shows the unprocessed seismograms of event 3 in which the later arrivals are not clear. Fig. 10 shows the TAPs for various values of V_a on an expanded scale which were obtained by keeping azimuth constant. As V_a is increased from 7 km/s to 55 km/s, depth phases, pP and sP, start appearing strongly around the V_a values which are close to that of the P phase (see Fig. 10).

Event 4

Fig. 11 shows the 20 channel seismogram of event-4 as recorded at GBA. TAPs for various values of V_a in an expanded time scale are shown in

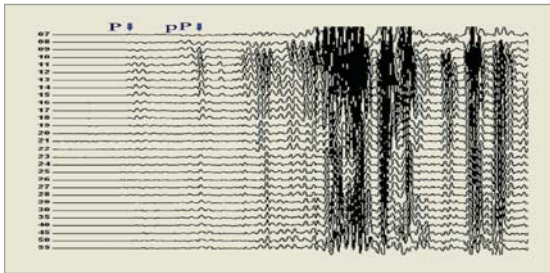


Fig. 7: TAP signals of event-2 for various apparent velocities (shown on the left). Depth phase pP is identified with the help of sScP phase (see figure 8). Plot duration is 65 s. prominent PP phase is also seen.

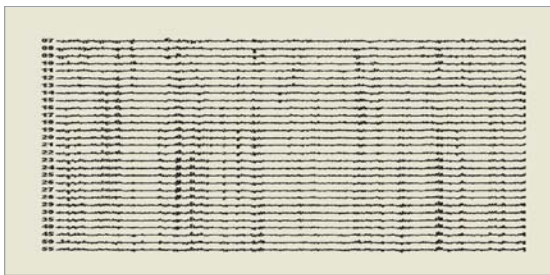


Fig. 8: TAP signals of event-2 around ScP arrival time, for various apparent velocities shown on the left. ScP and sScP phases arriving with large apparent velocities are clearly seen. Plot duration is 190 s.

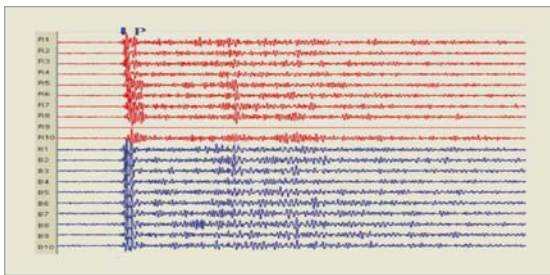


Fig. 9: Seismograms of event-3. Depth phases cannot be identified clearly. Plot duration is 260 s.

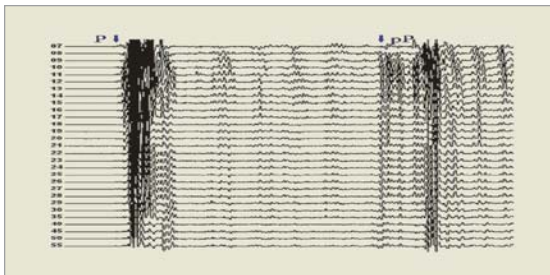


Fig. 10: TAP signals of event-3 for various apparent velocities are shown in expanded time scale. Depth phases pP and sP arriving with apparent velocity comparable to P wave may be seen very clearly. Plot duration is 90 s.

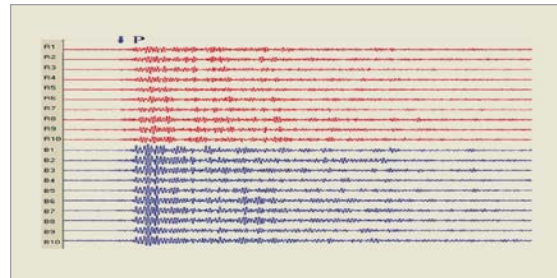


Fig. 11: Unprocessed seismograms of event-4 as recorded at GBA. Plot duration is 320 s.

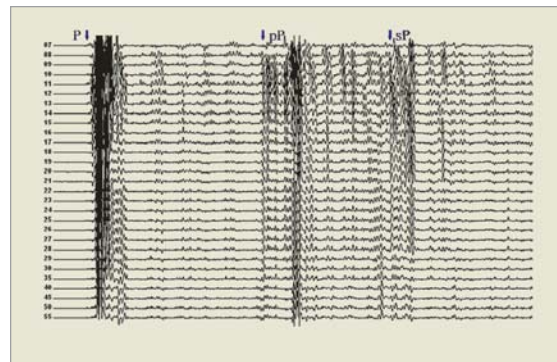


Fig. 12: TAP signals of event-4 for various apparent velocities are shown in expanded time scale. Depth phase pP arriving with apparent velocity comparable to P wave may be seen very clearly. However, though sP phase can be identified with reasonable accuracy, it apparently got merged with phases reflected from water surface. Plot duration is 45 s. PP phase is seen emerging strongly for low apparent velocity TAP signals.

Table I : Parameters of Sumatra events as reported by the USGS and obtained from the present study using SPIDER software.

Event No.	Date	Origin Time	USGS			GBA (SPIDER)			
			Lat	Lon	Mag	Depth	Lat	Lon	Depth
1	19-11-2010	215516.1	1.186	100.127	5.7	217	0.30	100.38	226
2	26-10-2010	234538.5	-2.360	099.853	5.5	25	-2.51	99.38	24
3	01-12-2010	005021.7	2.689	099.041	5.5	159	3.07	99.82	173
4	06-04-2011	140143.2	1.612	097.088	6.0	24	3.06	97.18	31

Fig. 12. Depth phase, pP, arriving with V_a comparable to P wave may be seen very clearly. Though sP phase can be identified with reasonable accuracy, it got merged apparently with the phases reflected from water surface. PP phase is seen emerging strongly in TAP signals for low V_a .

Conclusions

Seismic arrays play a significant role when it comes to estimation of apparent velocities or slownesses of various seismic phases and determination of azimuth to an event. These characteristics of a seismic array were used to demonstrate the efficacy of PcP, ScP and various depth phases including sScP phase in locating seismic events in Sumatra region with reasonable accuracy. Analysis of GBA short period seismograms pertaining to four events which occurred in Sumatra region demonstrated that estimated locations using the present method were in good agreement with those reported by United States Geological Survey keeping in view the fact that only a single array station data were used in the study.

Acknowledgements

We are thankful to our colleagues at Gauribidanur array for providing the digital waveform data and to the USGS for making available the event parameters at their website. We also thank Shri K. K. Bhuyan for helping us in preparing Fig. 1.

References

1. Birtill, J. W. and Whiteway, F. E. (1965). The application of phased array to the analysis of seismic body waves. *Proc. R. Soc. London, Ser. A*, 258, 421-493.
2. Dahlman, O. and Israelson, H. (1977). Monitoring underground nuclear explosions, Elsevier Scientific Publishing Company, Amsterdam, 440 pp.
3. Engdahl, E. R. and Selena Billington (1986). Focal Depth Determination of Central Aleutian Earthquakes, *Bulletin of the Seismological Society of America*, Vol. 76, No. 1, pp. 77-93
4. Forsyth, D. W. (1982). Determinations of focal depths of earthquakes associated with the bending of oceanic plates at trenches, *Physics of the Earth and Planetary Interiors*, 28, 141—160.
5. Jeffreys, Sir H. and Bullen, K.E. (1958). Seismological Tables. British Assoc. for Advancement of Science, Gray Milne Trust, London.
6. Mendiguren, J. A. (1971). Focal mechanism of a shock in the middle of the Nazca plate, *J. Geophys. Res.*76, 3861-3879.
7. Mowat, W.M.H. and Burch, R.F. (1974). Handbook for the stations which provide seismograms to the Blacknest Seismological Center, United Kingdom. Ref. No. AWRE/44/47/29, AWRE, Aldermaston, Berks.
8. Roy, Falguni (1984). Source depth estimation using multi-station waveform data, *Bull. Seism. Soc. Am.*, 74, 5, 1623-1643.
9. Roy, Falguni and Nair, G. J. (2005). A real time seismic monitoring and tsunami alert system. International workshop on external flooding hazards at NPP sites, Organized by AERB, NPCIL and IAEA, 29 August -02 September, 2005, Kalpakkam, India.
10. Weichert, D. H. (1975) Role of medium aperture arrays: The Yellowknife system, In: K. G. Beauchamp (Editor), *Exploitation of seismograph networks*, Nordhoff, Leiden, 167-196.

DNA Repair and Recombination Proteins (Dmc1 and Rad51) from Rice (*Oryza Sativa*)

Rajani Kant Chittela and Jayashree K. Sainis

Molecular Biology Division

Abstract

Homologous recombination is a process by which two DNA molecules interact physically and exchange the genetic information for maintaining the genome integrity and genetic diversity. Different proteins are involved in this process to carryout sequential biophysical and biochemical steps of this process. A special group of proteins called "Recombinases" are the central and crucial for this process as they mediate important steps like homology search, synapsis and strand exchange. In prokaryotes, RecA and in eukaryotes, RecA homologues, Rad51 and Dmc1 are important for this process. In this article, we report a brief over view of the work on rice DNA recombinases OsDmc1 (*Oryza sativa* Disrupted Meiotic cDNA1) and OsRad51 (*Oryza sativa* Radiation sensitive mutant 51). Both the proteins showed the hallmark properties of bonafied "Recombinase".

Introduction

DNA is the vital biomolecule, in which genetic information is stored in almost all living organisms. As living organisms are continuously exposed to different genotoxic agents, the template DNA is subjected to damage. DNA double-strand breaks (DSBs) produced during normal developmental stages due to the action of nucleases, errors in replication and due to exposure to radiation or genotoxic chemicals are repaired either by Homologous Recombination (HR) and Non-Homologous End Joining (NHEJ) (Symington, 2002). Though NHEJ is more predominant for DNA repair in eukaryotes, it frequently results in mutations as it is not error-free. Homologous recombination is relatively error-free and is a crucial process in all the living organisms including eukaryotes for maintaining the genomic integrity and also for generating genetic diversity, imperative for evolution.

The biochemical nature of homologous recombination and the genes involved in this process are well illustrated in the model prokaryotes such as *E. coli* (Kowalczykowski *et al.*, 1994). Homologous recombination involves identification of double strand breaks, generation of 3' overhangs, homology search in the undamaged partner, synapse formation between damaged and undamaged DNA molecules,

strand exchange between the paired DNA partners and resolution of Holliday junction to generate repaired DNA molecules without loss of genetic information. The DNA recombinases, implicated in homology search, pairing and strand exchange play a crucial role and are particularly interesting from the point view of structural and functional relationships. In *E. coli*, Recombinase-A (RecA) protein is well characterized.

In eukaryotes, homologous recombination is known to occur, predominantly during meiosis. Advancement of technologies for cloning and over-expression of eukaryotic genes and proteins have made it possible to investigate biochemistry of homologous recombination in eukaryotes (Fig.1). Two homologues of REC-A viz *RAD51* (Shinohara *et al.*, 1992) and *DMC1* (Bishop *et al.*, 1992) were identified first in yeast and later in mammals which perform a role similar to *E. coli* RecA with a significant help from other proteins belonging to *RAD52* epistasis group (Symington, 2002). The Rad51 protein mediates homologous recombination in mitosis and meiosis while Dmc1 is involved only in meiosis. *RAD51* orthologues have been identified in mouse and humans. Mutations in Rad51 gene in mice resulted in early embryonic lethality and inability of cell lines to grow *in vitro*. *ScRAD51*, in

S. cerevisiae is involved in repair of radiation induced DNA damage (Masson *et al.*, 2001; Symington, 2002). Dmc1 protein from yeast and human systems is also capable of mediating homologous pairing between a single strand and double stranded DNA. Dmc1 mutants are defective in reciprocal recombination, unable to process double-strand break (DSB) recombination intermediates and have inability to form normal synaptonemal complex (SC) which finally leads to arrest in meiotic prophase (Bishop *et al.*, 1992). The protein by itself was shown to exhibit a limited capacity for strand exchange (Hong *et al.*, 2001; Sehorn *et al.*, 2004).

As in other eukaryotes, homologous recombination is also crucial for generation of the genetic variability and also maintaining genomic integrity in plant systems. Several studies have been initiated to isolate the genes involved in homologous recombination in plants, especially genes for recombinases. Homologues of *DMC1* have been identified in *Lilium longiflorum*, *Arabidopsis thaliana* and *Oryza sativa*. *DMC1* mutants in arabidopsis showed random segregation of chromosomes in both male and female meiocytes. Recently it has been shown that homozygous parental lines can be derived from

heterozygous arabidopsis plant using reverse breeding approach by suppressing the *DMC1* expression (Wijnker *et al.*, 2012). Orthologues of *RAD51* gene have been identified in several plants like *Arabidopsis thaliana*, *Zea mays*, *Lycopersicon esculentum*, *Psycomitrella patens*. After gamma irradiation *RAD51* transcription levels in arabidopsis increased showing its involvement in double strand break repair. It was also shown that in arabidopsis *RAD51* was dispensable for vegetative growth but was required during meiotic recombination. *RAD51* paralogs in arabidopsis like *AtRAD51B*, *AtRAD51C* and *AtXRCC2* are known to play role in DNA repair and meiosis. In maize, Rad51 protein is involved in meiotic chromosome synapsis and segregation, supporting its involvement in meiotic homology search (Blueyard *et al.*, 2006). AtBrca2, a breast cancer susceptibility protein mediates the proper localization of AtRad51 and AtDmc1 during meiotic synapsis (Seeliger *et al.*, 2012).

The germline cells in plants are not predetermined as in case of animals. Any somatic cells can become a gametic cell. Plants are continuously exposed variety of environmental stresses, some of which may be genotoxic. DNA repair systems in higher plants have to be efficient and, therefore, interesting to investigate. Since DNA repair by non homologous end joining pathway (NHEJ) is more prone to mutations and genetic loss, homologous recombination assumes importance in maintaining genetic integrity in plants. Our investigation on OsDmc1 and OsRad51 is an important milestone in unraveling the biochemistry of homologous recombination in plants.

Characterization of Recombination Proteins Dmc1 and Rad51 from Rice

Previously two types of *OsDMC1* genes from japonica (AY123338 and AF375982) and indica (AY123340 and AY123339) cultivars of rice were sequenced in our lab. OsDmc1 Type A protein (~38.5 kDa) from Indica variety of rice was expressed in *E. coli* (Metkar *et al.*, 2004). Subsequently

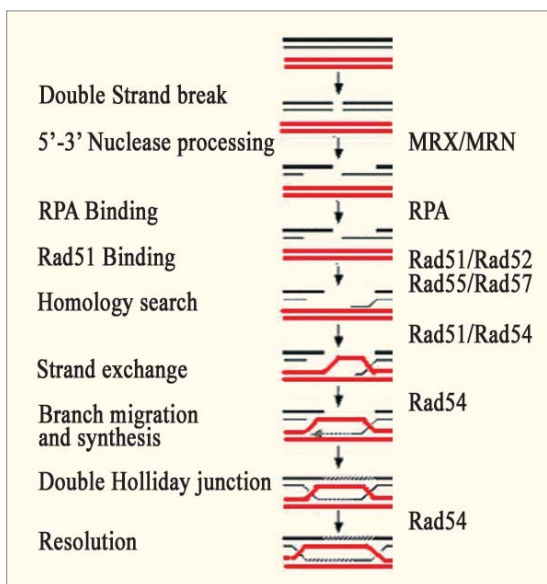


Fig.1: Different biochemical steps and proteins involved in DNA double strand break repair by homologous recombination

OsRAD51 cDNA from indica cultivar of rice was isolated, sequenced and overexpressed in *E. coli* and the purified proteins were characterized biochemically and compared in our lab.

Our studies with Electrophoretic Mobility Shift Assay (EMSA) using single stranded (ss) and double stranded (ds) DNA showed that *OsDmc1* has similar binding efficiency with ssDNA and dsDNA. *OsRad51* had more affinity towards ssDNA as compared to dsDNA. This property of *OsRad51* appears to be similar to the classical recombinases like *RecA*, which binds to preferentially to ssDNA. The binding to both the DNA substrates was not dependent of ATP, but required 5-10 mM Mg^{++} . Transmission Electron Microscopy (TEM) studies of nucleoprotein complexes showed that both of these proteins bind DNA and form helical filaments. *OsDmc1* and *OsRad51* both showed DNA dependent ATPase activity. Even though *OsDmc1* binds to both the DNA substrates, only ssDNA stimulated ATPase activity (Rajani Kant *et al.*, 2005). On the contrary *OsRad51* showed ATPase activity in presence of ss, dsDNA and even in absence of DNA. The ATPase activity of *OsRad51* was stimulated in presence of ssDNA (Rajanikant *et al.*, 2008).

Interestingly, both the proteins showed assimilation of complementary strands to form duplex molecules. *OsDmc1* also promoted assimilation of single strands into homologous super coiled duplexes leading to D-loop formation. This D-loop formation activity was promoted by non-hydrolysable ATP analog AMP-PNP and was not observed in absence of ATP or presence of ADP/ATP- γ -S. Under the same conditions *OsRad51* was unable to promote the D-loop formation. We also monitored DNA renaturation and strand exchange activities of *OsDmc1* (Rajanikant *et al.*, 2006) and *OsRad51* (Rajanikant *et al.*, 2008) in real-time using Forster Resonance Energy Transfer (FRET) (Figure 2). In case of *OsDmc1* the extent as well as the rate of renaturation was highest in conditions that contain ATP, but was significantly less in presence of AMP-PNP or ATP- γ -S. In absence of a nucleotide cofactor

it was several folds (~30 fold) lower. Interestingly, *OsRad51* mediated strand exchange reactions in presence and absence of ATP to the same extent. FRET changes were stable in both cases even after deproteinization step, suggesting that the results reflected stable events involving exchanges of homologous DNA strands. All these results, put together, suggest that *OsDmc1* and *OsRad51* proteins catalyze homologous renaturation as well as strand exchange activities, which are the classical hallmark properties of the bonafied *E. coli* recombinase. In parallel with our findings, it has been shown that *OsDmc1A* and *OsDmc1B* mediated robust strand exchange activity and form filamentous structures upon binding to DNA (Sakane *et al.*, 2008). Based on the rice DMC1 sequence information, DMC1 gene from maize was cloned and its functional domains like Walker motifs A and B, ssDNA binding site, dsDNA binding site and an

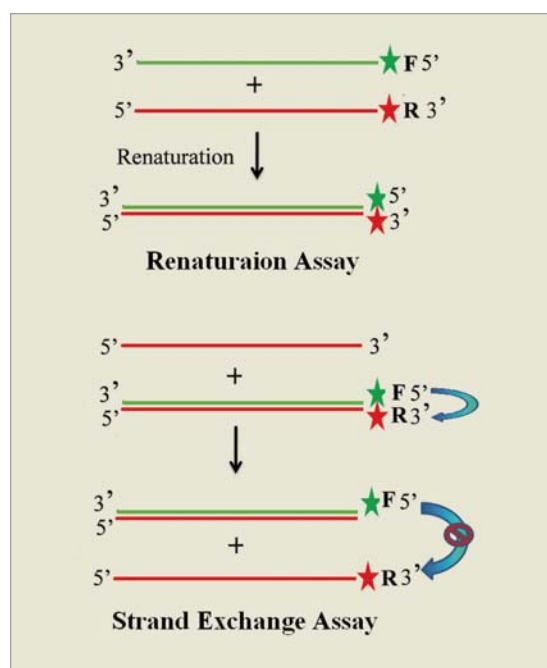


Fig. 2: Schematic representation of renaturation and strand exchange assay monitored by FRET. Fluoresceine (F) and Rhodamine (R) used as a FRET pair in these assays. FRET in case of renaturation as both the dyes are juxtaposed after annealing and loss of FRET in case of strand exchange as F and R were separated as result of strand exchange was monitored.

interface domain responsible for multimer formation were mapped (Etdali et al., 2011).

Conclusion and Future Directions

Eukaryotic DNA is organized into higher order structures called "chromatin" composed of histone and non-histone proteins. It has been shown in yeast and mammalian systems that upon DNA damage chromatin remodeling has to occur for facilitating the DNA repair and recombination. However, this aspect is less explored in plant systems. Recently, we have observed that exposure of wheat seedlings to ⁶⁰Co- γ radiation induced differential acetylation and phosphorylation of Histones H3 and H4 which would play important role in ATP independent events of chromatin remodeling in post irradiation DNA repair (Raut and Sainis, 2011). We also isolated and characterized an ATP dependent chromatin remodeling complex, which showed histone trans transfer activity from wheat seedlings (Raut et al, 2011). All these studies open up new vistas in the field of DNA repair and recombination in plants (Chittela RK and Sainis JK, 2010). In future it would be important to study proteins involved in DNA repair recombination machinery of plants and investigate their functions *in vitro* and *in vivo*.

These studies would unravel the newer possibilities of targeting genes in transgenic plants and understand their exact role in DNA repair and recombination in plants. Apomixis is a process by which plants produce embryos without going through the routine fertilization and meiosis. Though apomixis is known from decades, recently it has gained a considerable importance as this process would be able to maintain the hybrid vigour by avoiding the sexual reproduction involving recombination of parental traits. By suppressing the genes like DMC1 during meiotic recombination and over expression of genes responsible for apomixis, seeds can be produced which would maintain parental hybrid vigor. However, this calls for more basic research at genetic and biochemical level to understand the molecular mechanisms of DNA repair and recombination in plants.

Acknowledgements

Our sincere thanks to Dr. S. K. Apte for support and encouragement of this activity. Our thanks also due to Dr. Michael Melzer, Head, Structural Biology Group, IPK, Gatersleben, Germany and his research team for their support during transmission electron microscopy experiments.

References

1. Bishop, D.K., Park, D, Xu, L, and Kleckner, N. (1992) *DMC1*: A meiosis-specific yeast homolog of *E. coli recA* required for recombination, synaptonemal complex formation, and cell cycle progression. *Cell* 69, 439-456.
2. Bleuyard, J.Y., Maria, E., Gallego, B and White, C.I. (2006) Recent advances in understanding of the DNA double-strand break repair machinery of plants *DNA Repair* 5, 1–12.
3. Chittela R.K and Sainis J.K. (2010) Plant DNA Recombinases: A Long Way to Go. *J Nucleic Acids*. 2010: 646109.
4. Etedali F, Baghban Kohnehrouz B, Valizadeh M, Gholizadeh A, Malboobi M.A. (2011) Genome wide cloning of maize meiotic recombinase Dmc1 and its functional structure through molecular phylogeny. *Genet Mol Res*. 10:1636-1649.
5. Hong, E.L., Shinohara, A. and Bishop, D.K. (2001) *Saccharomyces cerevisiae* Dmc1 protein promotes renaturation of single-strand DNA (ssDNA) and assimilation of ssDNA into homologous super-coiled duplex DNA. *J Biol Chem* 276, 41906-41912.
6. Kowalczykowski, S. C., Dixon, D. A., Eggleston, A. K., Lauder, S. D., and Rehrauer, W. M. (1994) Biochemistry of homologous recombination *E. coli*. *Microbiol. Rev.* 58, 401-465.
7. Masson, J. Y. and West, S. C. (2001) The Rad51 and Dmc1 recombinases: a non-identical twin relationship. *Trends Biochem. Sci.* 26:131-136

8. Metkar, S.S., Sainis, J.K. and Mahajan, S.K. (2004) Cloning and characterization of the DMC1 genes in *Oryza sativa*. *Curr.Sci.* 87: 353–357.
9. Rajani Kant C, Rao, B.J. and Sainis J. K. (2005) "DNA binding and pairing activity of OsDmc1, a recombinase from rice". *Plant Molecular Biology* 57, 1-11.
10. Rajanikant, C., Kumbhakar, M., Pal, ., Rao, B.J and Sainis, J.K. (2006) "DNA strand exchange activity of rice recombinase OsDmc1 monitored by fluorescence resonance energy transfer and the role of ATP hydrolysis". *FEBS J* 273: 1497-1506.
11. Rajanikant, C., Melzer, M., Rao, B.J and Sainis, J.K. (2008) Homologous recombination properties of OsRad51, a recombinase from rice. *Plant Molecular Biology*, 68: 479-491.
12. Raut V.V and Sainis J.K. (2011) ⁶⁰Co- γ radiation induces differential acetylation and phosphorylation of histones H3 and H4 in wheat. *Plant Biology*, 14: 110-7.
13. Raut Vishal, Pandey Shashibhal and Sainis Jayashree (2011) Histone Octamer Trans-transfer -A Signature Mechanism of ATP Dependent Chromatin Remodeling Unraveled in Wheat Nuclear Extract. *Annals of Botany*, 108: 1235-1246.
14. Sakane I, Kamataki C, Takizawa Y, Nakashima M, Toki S, Ichikawa H, Ikawa S, Shibata T, Kurumizaka H (2008) Filament formation and robust strand exchange activities of the rice DMC1A and DMC1B proteins. *Nucleic Acids Res.* 13:4266-76.
15. Seeliger K, Dukowic-Schulze S, Wurz-Wildersinn R, Pacher M, Puchta H (2012) BRCA2 is a mediator of RAD51- and DMC1-facilitated homologous recombination in *Arabidopsis thaliana*. *New Phytol.* 193:364-375.
16. Sehorn, M.G., Sigurdsson, S., Bussen, W., Unger, V.M. and Sung, P. (2004) Human meiotic recombinase Dmc1 promotes ATP-dependent homologous DNA strand exchange. *Nature* 429, 433-437.
17. Shinohara, A., Ogawa, H. and Ogawa, T. (1992) Rad51 protein involved in repair and recombination in *Saccharomyces cerevisiae* is a RecA-like protein. *CELL* 69: 457-470
18. Symington, L. S. (2002) Role of *RAD52* epistasis group genes in homologous recombination and double strand break repair. *Microbiology and Molecular Biology Reviews* 66: 630-670.
19. Wijnker E, van Dun K, de Snoo CB, Lelivelt CL, Keurentjes JJ, Naharudin NS, Ravi M, Chan SW, de Jong H, Dirks R (2012) Reverse breeding in *Arabidopsis thaliana* generates homozygous parental lines from a heterozygous plant. *Nat Genet.* 44:467-470.

Recovery of Cesium from High Level Liquid Nuclear Waste by an Advanced Polymer Composite

Lalit Varshney and V.Venugopal

Radiochemistry and Isotope Group

and

Amar Kumar, Tessy V. and S.D. Mishra

Nuclear Recycle Group

Abstract

Recovery of ^{137}Cs is one of the important steps in safe and effective management of High Level Liquid Waste (HLLW). Precipitation, solvent extraction and ion exchange are the prominent processes used for ^{137}Cs separation. Ion exchange processes, based on inorganic ion-exchangers, have several advantages like high radiation stability of material, high selectivity of Cs over other constituent present in the waste, lower volume of secondary waste generation, simple operational procedure etc. Ammonium molybdophosphate (AMP) is a well established inorganic exchanger for selective separation of Cs from HLLW. However, it cannot be used as such for column operations because of its microcrystalline nature. Use of other polymer based systems have known technical operational problems. ALIX (Advanced Lyophilic Ion-exchanger), recently developed at BARC, is an engineered form of composite ion-exchanger, observed to be useful in separation of Cs^+ from highly acidic nuclear waste at demonstrable scale.

Introduction

^{137}Cs ($T_{1/2} = 30$ years) is one of the principal radionuclides produced during the fission of ^{235}U in nuclear reactors. It is a major source of radiation in HLLW generated after the reprocessing of spent nuclear fuel. Separation of Cs from HLLW, reduces radiation exposure during the vitrification process and prevents thermal deformation of conditioned waste matrix during storage. Separation of ^{137}Cs would also markedly reduce its volatility during vitrification, extent of migration from the vitrified mass in repository, operational, transportation and storage cost. In addition, ^{137}Cs finds applications as a radiation source for food preservation, sterilization of medical products, brachytherapy, blood irradiation, hygienization of sewage sludge etc. The use of ^{137}Cs in place of ^{60}Co ($T_{1/2} = 5.2$ years) will also reduce the shielding requirement, frequency of source replenishment and ease the handling / transportation of radioactive source(1-4). In the new polymer composite, 80%AMP is blended with an inert polymer substrate namely a polysulfone. The inert polymer support is stable in 3-5 M Nitric acid

as well as in 1-3 M NaOH, has high thermal and radiation stability and does not reduce the ion exchange capacity of encapsulated AMP. Evaluation of ALIX as an ion-exchanger for recovery of Cs from simulated HLLW shows that 2.42Ci of ^{137}Cs can be loaded on one gram of ALIX without any operational problem. Loaded Cs can be recovered from the column by dissolving it in 1.0M NaOH solution. It can be further purified by passing the dissolved AMP solution through Resorcinol-Formaldehyde (RF) ion-exchange column. On the basis of these experimental results, which were carried out on an Engineering Scale Experimental Facility, a conceptual process flow sheet has been developed for recovery of Cs from HLLW on demonstration scale. The polymer composite has also given new directions for development of various other encapsulated liquid/solid extractants useful for extracting other radionuclides of interest and Rare Earths. The composite has flexibility of modifications to meet various requirements for successful implementation of the separation process.

Characteristics and application of ALIX

ALIX is an engineered form of composite ion exchanger in which AMP is blended with inert polymer substrate which is stable in nitric acid as well as NaOH and does not reduce the ion exchange capacity of encapsulated AMP. ALIX has fibrous internal structure containing AMP crystals, surrounded by an outer layer of polymer and AMP composite having thickness of 15-25µm. The surface pores on the layer have sizes of the order of 100-300nm (Fig. 1). The morphological structure of the composite is responsible for controlling exchange kinetics. The results given here are for the optimum bead structure having 45-49% void volume and 35-40 min. equilibrium time. In the bead structure, AMP crystallites are not coated by the substrate and are just embedded in the cavities, thus available for faster Cs⁺ exchange as well as instant dissolution by Alkali.

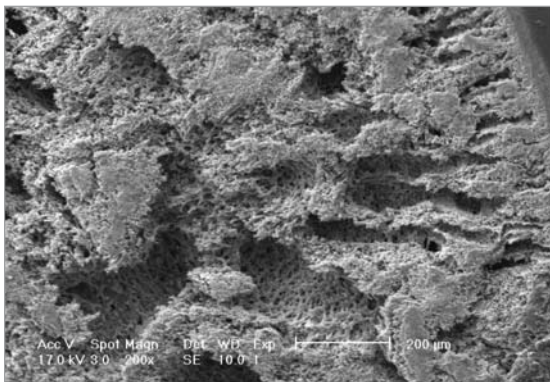


Fig. 1: Cross sectional view of ALIX spherical bead as seen under SEM

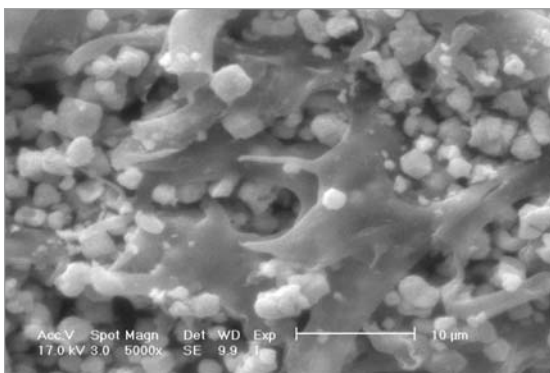


Fig. 2: Distribution of AMP inside the ALIX

The formation process of ALIX is very simple, environmentally safe and economical and is based on nonsolvent induced phase separation technique. The technology for the production of large quantity of ALIX has been indigenously developed and ingredients required for its preparation is locally available.

Evaluation of ALIX in bench scale experimental facility

ALIX was evaluated for recovery of Cs⁺ from typical PHWR simulated HLLW, generated during the reprocessing of spent fuel having burn up of 7000 MWD/Ton. Concentration of various constituents in simulated waste is given in Table 1. It shows that U, Na Fe and Cs are the major constituents present in the waste. The simulated waste containing ¹³⁴Cs tracer was passed through a 1.5 litre stainless steel column containing ALIX beads at a rate of 4.5 bed vol/h. Concentration of ¹³⁴Cs in the effluent was determined by Gamma counter equipped with NaI(Th) detector. 110 bed volumes of HLLW was passed through the column to get complete breakthrough. Exchange kinetics of Cs⁺ present in simulated HLLW with ALIX was obtained by

Table 1: Typical composition of HLLW

Elements	Conc. (g/L)	Elements	Conc. (g/L)
Fe	0.72	Mn	0.426
Cr	0.119	U	6.34
Ni	0.107	Sr	0.031
Na	5.5	Zr	0.004
K	0.224	Mo	0.137
Mn	0.426	Ba	0.064
U	6.34	La	0.18
Sr	0.031	Ce	0.06
Zr	0.004	Pr	0.09
Mo	0.137	Nd	0.12
Sm	0.0855	Cs	0.315 (9.135 Ci/L)
Y	0.06	Acidity (HNO ₃)	3.05 M

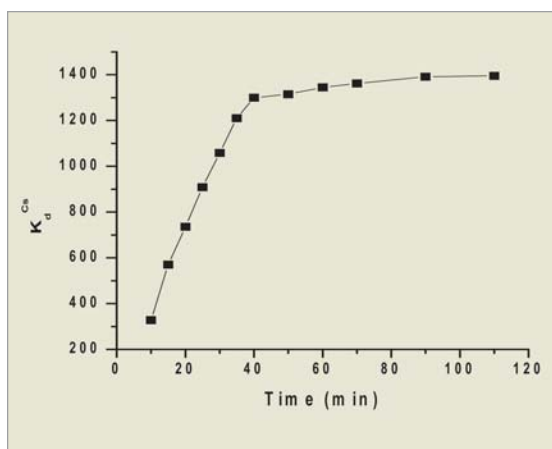


Fig. 3: Sorption kinetics of Cs⁺ from Simulated HLLW

determining the distribution coefficient K_d^{Cs} at different interval of time. K_d^{Cs} is defined in equation 1. Fig. 3 shows that initially K_d^{Cs} increases with increasing time of equilibration. Equilibrium was achieved in 40 minutes.

$$K_d^{Cs} = \left(\frac{A_i - A_f}{A_f} \right) \frac{V}{g} \quad \text{---eq. 1}$$

Where as A_i = Initial Cesium activity, A_f = final Cesium activity, V = volume of solution containing Cesium, g = dry weight of polymer composite.

Dynamic exchange capacity of ALIX in this experimental condition was found to be 0.34 meq/g.

Selective dissolution of AMP from ALIX column

During the exchange Cs⁺ becomes a part of AMP crystal. Regeneration of AMP is not energetically favourable because this exchange is accompanied by phase transition that leads to decrease in lattice energy. This would lead to use of higher conc. of NH_4SO_4 for regeneration. Therefore, AMP was selectively dissolved from the ALIX in 1.0M NaOH. Dissolution proceeds due to following chemical reaction:

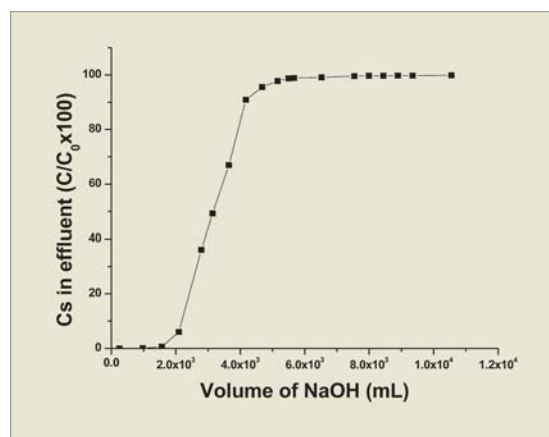
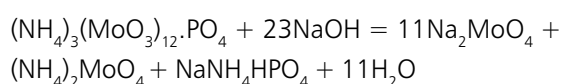


Fig. 4: Variation of [Cs⁺] in the effluent with dissolution of AMP in the ALIX



Batch dissolution study shows that 4.156 moles of NaOH is required to dissolve 0.180 moles of AMP loaded in the ALIX column. 1.0M NaOH is the threshold concentration required to achieve optimum dissolution rate. Instantaneous dissolution takes place at room temperature. The extent of dissolution was measured by determining the concentration of Cs⁺ and pH of dissolved solution. The process is shown in Fig 4. The Pictorial view of dissolution process of AMP from the ALIX is shown in Fig. 5.

Regeneration of ALIX column using 3 M NH_4SO_4 was also explored. In this case, only 70 % of loaded Cesium could be eluted. Moreover, separation of Cesium from Ammonium sulphate solution is a cumbersome process. Therefore, selective dissolution of AMP from ALIX is more desirable.



Fig. 5; Dissolution process of AMP from ALIX.

Recovery of Cs from dissolved AMP solution

Resorcinol Formaldehyde Resin (RF) was employed for selective separation of Cs⁺ from dissolve AMP solution. The hydroxyl group attached to benzene ring of the RF resin is a weak acid and dissociates at higher PH. It is highly selective for Cs⁺ due to its low hydrated ionic radius as compare to Na⁺. Fig.6 shows sorption isotherm of Cs⁺ on RF resin. This isotherm was obtained by varying the Cs⁺ concentration in aqueous phase from 5 x 10⁻⁴M to 5 x 10⁻² M at 12.5 pH. Isotherm indicates that Cesium exchange capacity (CEC) of RF resin is 1.53 meq/g. RF resin is a regenerative types of exchanger on which Cs⁺ was loaded at >12.5 pH. Once column is saturated with Cs⁺, it can be recovered by eluting with 0.5M HNO₃ solution. Cs⁺ rich solution can be used as radiation source after immobilizing in solid inert matrix

The results of the study on ALIX system indicate that ALIX is a suitable polymer composite for separation of Cs⁺ from high level acidic liquid waste from spent fuel.

Conclusions

The results of the present study indicate that it is possible to separate ¹³⁷Cs on engineering scale from HLLW using ALIX polymer composite.

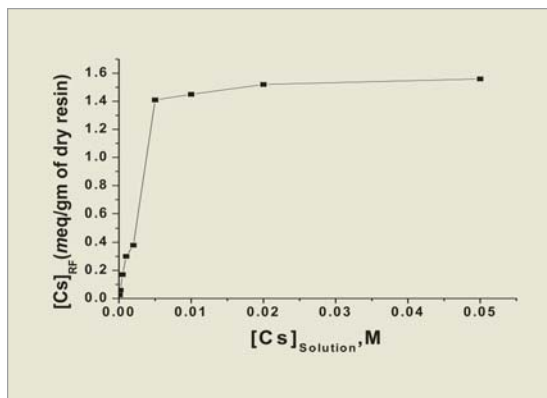


Fig. 6: Equilibrium sorption isotherm for Cs⁺ on RF resin

Acknowledgement

The authors are grateful to Dr.P.K. Wattal , Dr. K.L. Ramakumar, Dr. Gursharan Singh, for encouragement and Dr. Dr. J.G. Shah for SEM photographs and useful discussions.

References

1. Preparation of PAN based absorber for separation of Cesium and Cobalt from radioactive wastes. A Nilchi, H. Atashi, A.H. Javid, R. Saberi, *Applied Radiation and Isotopes* 65(2007)482-487.
2. Evaluation of ammonium molybdophosphate-polyacrylonitrile (AMP-PAN) as a cesium

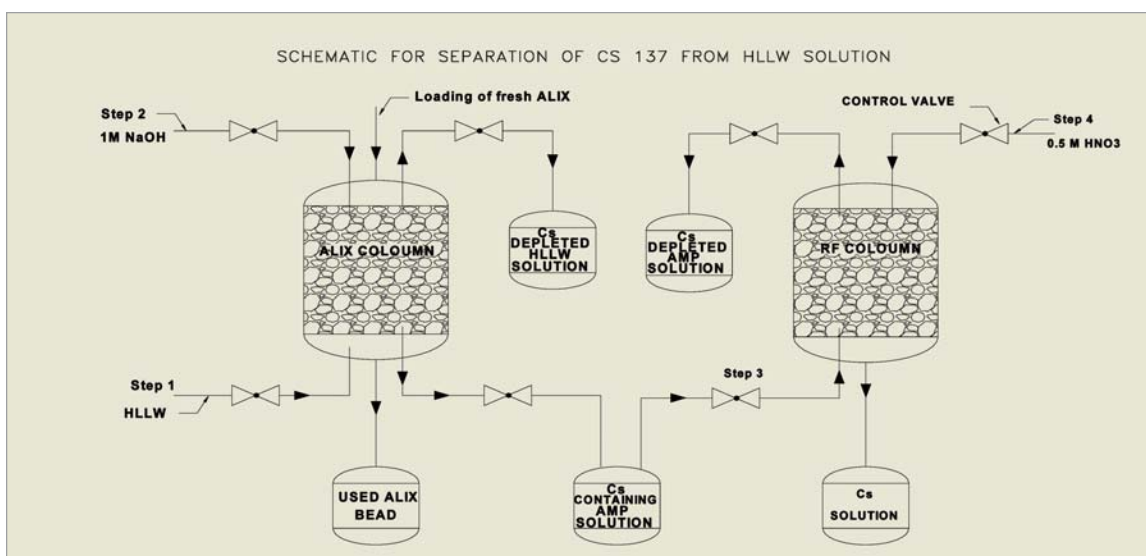


Fig.7: Schematic for separation of ¹³⁷Cs from HLLW

selective sorbent for the removal of ^{137}Cs from acidic nuclear waste solution T. J. Tranter, R. S. Herbst, T. A. Todd, A. L. Olson, H. B. Eldredge. *Advances in Environmental Research*, Volume 6, Issue 2, March 2002, Pages 107-121

3. Evaluation of polymer inclusion membranes containing crown ethers for selective cesium separation from nuclear waste solution. P.K. Mohapatra, D.S. Lakshmi, A. Bhattacharyya, V.K. Manchanda, *Journal of Hazardous Materials*, Volume 169, Issues 1-3, 30 September 2009, Pages 472- 479.
4. Selective extraction of cesium ion with calix[4]arene crown ether through thin sheet supported liquid membranes. *Journal of Membrane Science*, Volume 187, Issues 1-2, 15 June 2001, Pages 3-11). K. Kim, J. S. Kim, Y. G. Shul, K. W. Lee, W. Z. Oh.

Forthcoming Conference

1st National Conference on Micro and Nano fabrication

(21 to 23) January, 2013

The micro and nano fabrication technology is an important bridge to take findings of nano sciences to the real world. The 1st *National Conference on Micro and Nano Fabrication Technologies*, to be organized by Central Manufacturing Technology Institute aims to propagate micro and nano fabrication activities by way of providing an inspiring platform for exchange of research advances and findings. This conference will focus on areas of micro and nanofabrication technologies. The conference will be held in CMTI, Bengaluru, India during January 21-23, 2013.

Scope

The conference covers following broad areas / activities:

- Micro/Nano Machining
- Nano Finishing
- Micro/Nano Patterning
- Micro/Nano Products
- FIB and e-beam based Machining
- Laser based Micro Machining
- Surface Engineering and Tribo-coating Technology
- Nano Materials Characterization
- Nano Metrology

Important Dates

Abstract submission: 30 Sep, 2012

Notice of abstract acceptance : 5 Oct., 2012

Full manuscript submission: 25 Oct. 2012

Notice of full manuscript acceptance: 5 Dec, 2012

Final manuscript submission: 15 Dec., 2012

Last date of Registration for

Pre-Conference 20 Dec., 2012

Registration

Registration can be made by filling up the registration form available at CMTI official website and sending the same to the organizing secretary. Payment may be made in the form of *DD/* Pay Order, payable to CMTI at Bangalore. *DD/* Pay order may kindly be Chairman: Mr. B.R.Satyan, Director, CMTI posted to P.V. Shashikumar, Joint Director, Central Manufacturing Technology Institute (CMTI), Tumkur Road, Bangalore - 560022

E-mail: pvs@cmti-india.net.

Website : www.cmti-india.net

Performance Study of Indigenously Developed CsI-Photodiode Linear Array Detectors for X-Ray Baggage Scanning Application

Anita Topkar, Arvind Singh, P.K.Mukhopadhyay and C.K.Pithawa

Electronics Division

and

Umesh Kumar and Lakshminarayana Y.

Isotope Application Division

Abstract

Linear array detectors with 16-element PIN photodiode coupled to a 16 element CsI array of geometry matching to the photodiode elements has been indigenously developed. These arrays have been characterized at various X-ray intensities by varying the current and voltage setting of the X-ray source and by incorporating Cu, Al and SS filters in the path of X-rays. The results of the performance tests confirm the suitability of the detectors for X-ray baggage scanning applications.

Introduction

Silicon PIN photodiode coupled to scintillator are used for several research applications involving measurement of energy of high energy charged particles and photons. Nowadays, these detectors are being increasingly used for X-ray imaging systems for security inspection, industrial tomography, and medical applications. For example, modern X-ray baggage scanning systems and container scanning systems use linear array detectors made of suitable scintillators coupled to a silicon photodiode array. In a solid-state detector for X-ray detection, a p-i-n (PIN) photodiode is used as a photosensor of visible light from the scintillator.

Scintillator coupled photodiode detectors allow compact detector systems operating at a much lower voltage compared to their counterpart, scintillator-PMT type of detectors. Commercially available detectors used for such applications incorporate segmented scintillators with dimensions suitable with the corresponding photodiode elements. It is possible to use scintillators of different atomic number, density and element length, which allows operation in the energy range from about 100 keV to 9MeV X-ray/LINAC based systems.

Cesium iodide (CsI) and cadmium tungstate (CdWO_4) are the most commonly used scintillators in these detectors.

Electronics Division, BARC has developed the technology for the fabrication of PIN photodiodes using a 4" integrated circuit processing facility [1]. The performance of these photodiodes for γ -ray spectroscopy was also demonstrated by coupling to CsI scintillator [2]. As a next step, 16-element linear array detectors suitable for X-ray baggage scanning applications have been developed. In this article, we present detailed experimental results of the detector response to the incident X-rays for different X-ray intensities.

Design and Fabrication Technology

The fabricated and packaged photodiode array is shown in (Fig.1).

The design of photodiode has been carried out to have geometries similar to those for commercially available photodiode array detectors for baggage scanning applications. The photodiode mask for fabrication of silicon wafers was designed to incorporate 16 elements with element geometry of 2.5 mm x 2.15 mm and element pitch of 2.5mm. A four layer mask defining p+ implant, contact,

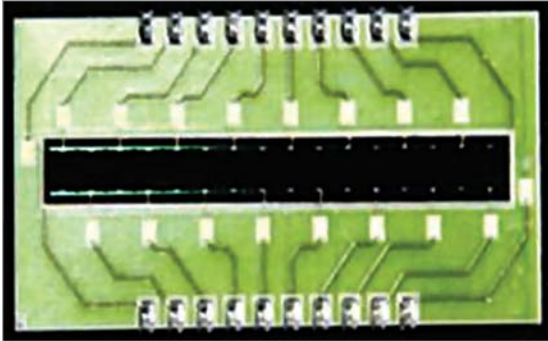


Fig. 1: Fabricated and packaged 16-element photodiode array

metal and passivation layers has been used for fabrication of these photodiodes. The 16-element photodiode arrays have been fabricated using a custom technology derived from integrated circuit technology. High purity silicon wafers (resistivity $> 3 \text{ k}\Omega\text{-cm}$) have been used as a starting material. Processes used for integrated circuit fabrication such as silicon oxidation, ion implantation, aluminum metallization, lithography, etc, have been used for fabrication of photodiodes. For the PIN photodiode, it is important to make p-layer as shallow as possible. In order to achieve shallow junction, the optimum conditions of ion implantation such as dose and energy, thickness of SiO_2 screen oxide and implant annealing conditions have been used. The fabrication process was tuned to realize photodiodes with very low dark currents of about 10 pA/element (with element area – 5.375 mm^2). The capacitance per element was about 50 pF at 10 mV bias. Low dark currents are essential to reduce the electronic noise of the photodiodes. The fabrication process is schematically shown in the flow chart in (Fig. 2.) After completion of wafer processing, the wafers are diced and the individual arrays are packaged on ceramic substrates. The contact to each element is provided by wire bonding using a $25 \mu\text{m}$ diameter aluminum wire. Before coupling to scintillator, dark current of each element of the photodiode array has been measured to ensure that the dark currents of all elements are low and are uniform. The measurements with light were also carried out to measure the responsivity and to check the uniformity of optical response. The optical response was

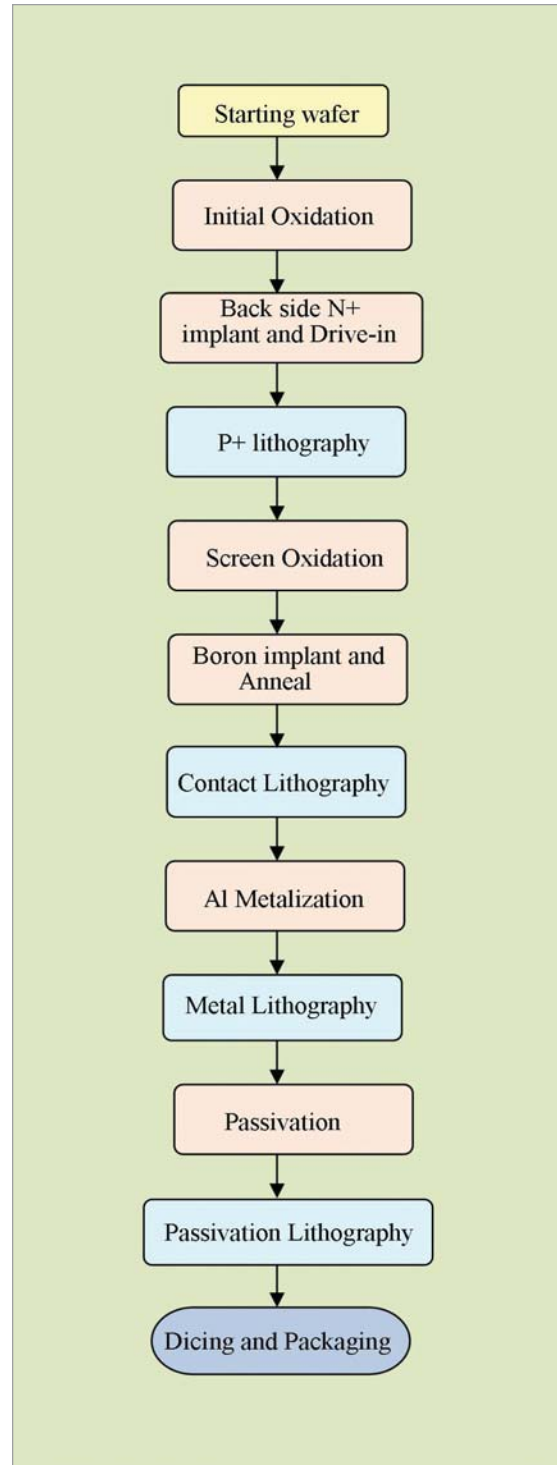


Fig. 2: Process flow for fabrication of photodiodes

observed to be uniform and showed a responsivity of 0.41 A/W at 630 nm wavelength. The photodiode array has been optically coupled to a 16-element CsI scintillator array. The thickness of the scintillator array was chosen for 140 keV X-ray

operation. (Fig. 3) shows the picture of 16-element CsI coupled photodiode array. The overall dimension of the packaged array is 4.8 cm x 2.0 cm. The pixel size of CsI matches with the corresponding element of photodiode (2.5 mm x 2.15 mm). The pixels of CsI are separated by a separator to prevent cross talk. The photodiodes have been tested for dark current after coupling to scintillator to verify that there is no significant degradation of electrical performance during the process of gluing the CsI to photodiodes. The typical dark currents of each pixel before and after coupling to CsI at a reverse voltage of 10 mV are as shown in (Fig. 4). The mean value and spread of the per-coupling dark current and post-coupling dark current are 8.2 pA ± 1.3 pA and 8.7 pA ± 1.5 pA respectively.

Experimental setup for measurement of detector response with X-rays

The measurement of linear array detector response has been obtained by using an X-ray beam impinging on the scintillator. During the measurements, the detector and the readout electronics were enclosed in a lead box. (Fig. 5) shows the experimental arrangement. Fig. 6 shows the detector along with electronics for simultaneous measurement of current in 16 channels. The lead box was designed to have a collimator on the front face to expose only the 16 element scintillator. Two types of measurements were performed:

a) An electrometer has been used to measure the current generated in the photodiode elements. The electrometer provides a voltage output proportional to the current under measurement (10 mV/nA).

The electrometer was located at a close distance with the photodiode array and the voltage output was measured using a high end DMM outside the X-ray source room.

b) Simultaneous measurement of response of all 16 elements using a 16-channel current to voltage converter (Gain of 10⁶ V/Amp or 1 mV/nA), S/H and analog multiplexer. The analog multiplexer provides serial output of all 16 channels after a

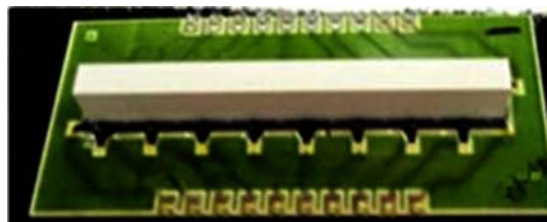


Fig. 3: CsI coupled photodiode linear array

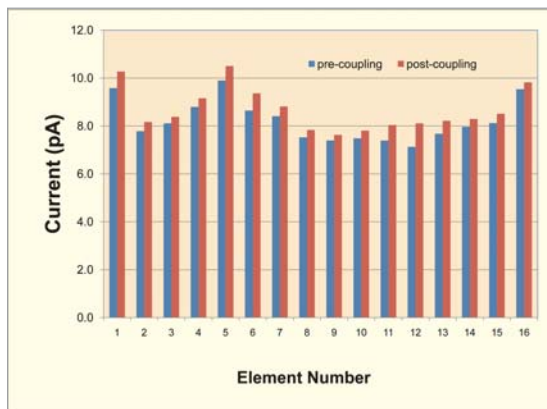


Fig. 4: Dark current for 16 elements before and after coupling CsI to photodiode



Fig. 5: Experimental arrangement for testing the detector with X-ray source

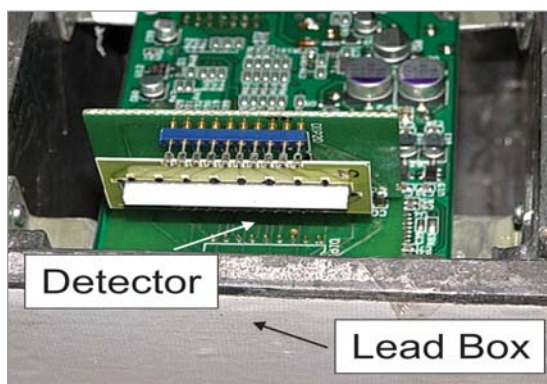


Fig. 6: Detector with electronics for simultaneous measurement of current in 16 elements

trigger signal. The X-ray response has been studied for 80 keV, 100 keV and 140 keV X-ray tube settings and for currents of 4 mA, 6 mA and 8 mA.

Detector response with X-rays

The response of the CsI-photodiode array to X-rays at three different energies (80 keV, 100 keV and 140 keV) and different current settings (4 mA, 6 mA and 8 mA) is as shown in (Fig.7) (a), (b) and (c) respectively. The elements are numbered from left to right in these figures and subsequent figures. As expected, the current generated in the elements and therefore the output voltage increases as the energy and current of the X-ray tube is increased. The last element (No 16) was not exposed completely through the collimator and therefore shows reduced response compared to other 15 elements. The X-ray intensity increases linearly with current. Hence, it is expected that the current generated in the photodiodes would scale accordingly when the current is increased from 4 mA to 6 mA or 8 mA at a particular voltage setting. The actual output voltage observed at 4 mA and 6 mA at 140 keV and the expected output voltage calculated from the 8 mA/140 keV data is plotted in (Fig.8). As can be seen there is good agreement in the calculated and the experimentally observed data.

The X-ray intensity varies as a square of X-ray tube voltage. Hence if the tube voltage is changed from 80 keV to 100 keV, it is expected that the output voltage will increase by a factor of $1.5625 (= (100/80)^2)$. Therefore the experimentally observed data for 100 keV should show an increase by a factor of 1.5625 when compared to the data obtained at 80 keV. Similarly, it is expected that the measured output voltages at 140 keV should scale by a factor of 3.0625 compared to the output voltages at 80 keV.

Fig. 9 shows the comparison of the output voltages for each element at 100 keV and 140 keV. The data obtained at 80 keV is scaled by a factor of 1.5625 for 100 keV data and by a factor of 3.0625 for 140 keV data. As can be seen, the actually observed

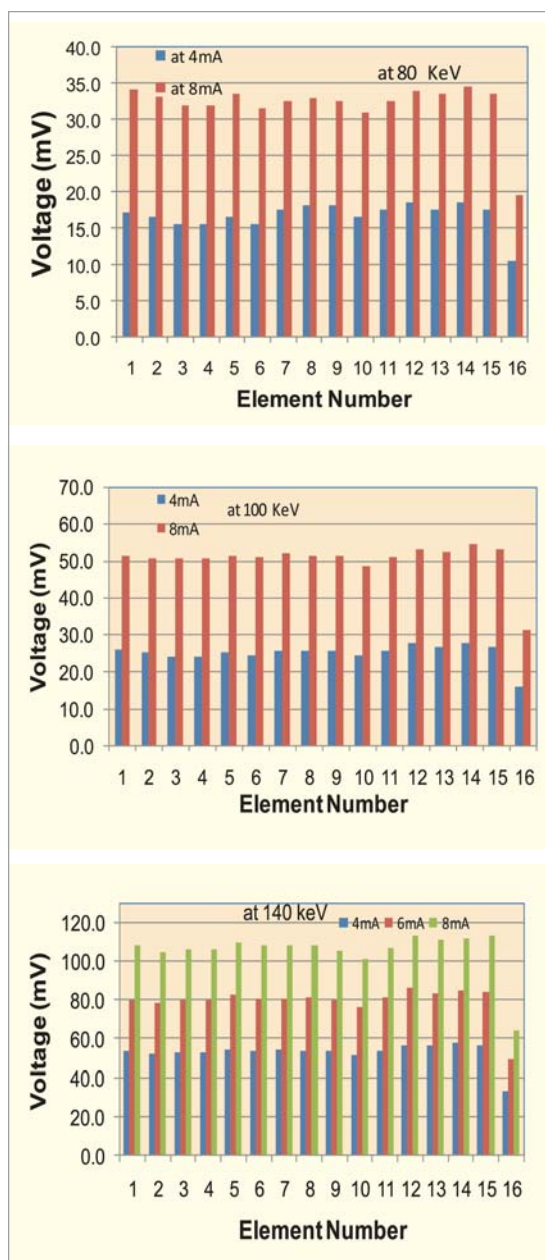


Fig. 7: Typical Output voltage at
(a) 80 keV/4 mA, 8 mA,
(b) 100 keV/4 mA, 8 mA,
(c) 140 keV/4 mA, 6 mA, 8 mA

element voltages are in close agreement with the estimated element voltages. The element to element variation of the output voltage for three different current settings of X-ray tube (4 mA, 6 mA and 8 mA) is shown in Fig.10. As can be seen the output response is quite uniform within elements. The experimentally observed variation is within $\sim \pm 7.5\%$, which is acceptable.

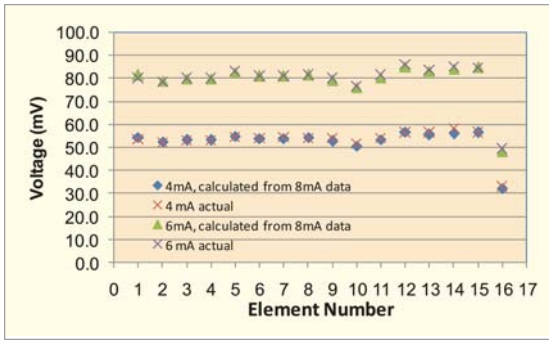


Fig. 8: Comparison of calculated and experimentally obtained values of output voltage

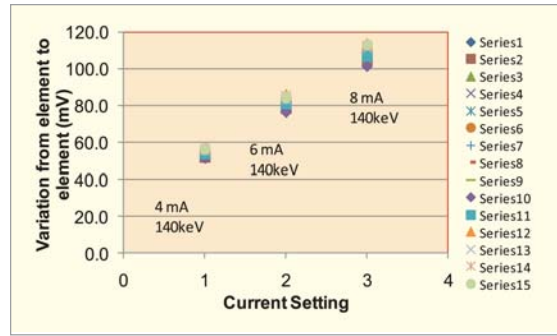


Fig. 10: Output response variation from element to element for 140V/4mA, 6mA, 8mA setting

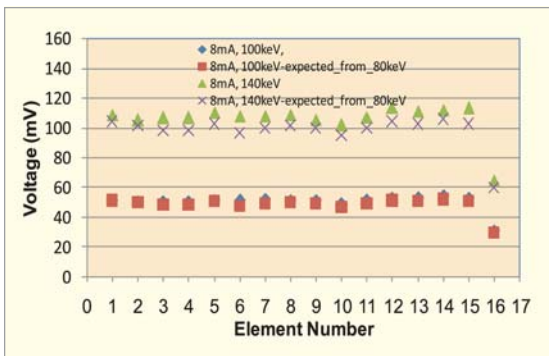


Fig. 9: Experimentally obtained output voltages at (i) 100 keV, 8 mA, (ii) 140 keV, 8 mA and calculated voltages from 80 keV, 8 mA data

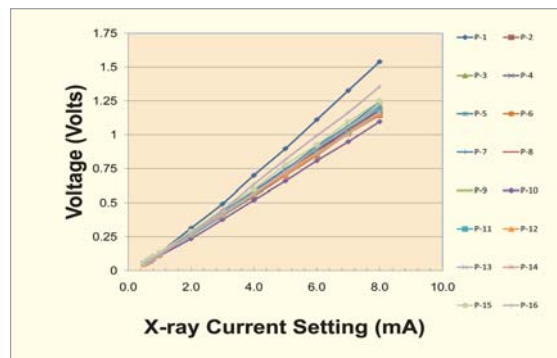


Fig. 11: Variation of output voltage of each element for different X-ray current settings at 140 keV

The linearity of the output response for a current setting between 0.5 mA to 8 mA was verified by measuring the individual element response. For this purpose, the element was connected to an electrometer and the output voltage proportional to current was measured by setting the electrometer at a fixed range. The output voltage of the electrometer for the fixed gain was 10 mV/nA. The individual element voltages are plotted at a X-ray tube setting of 0.5 mA to 8 mA at 140 keV (Fig. 11).

The plot shows that the measured variation of output response is linear with the X-ray intensity in the current range of 0.5 mA to 8 mA. The output voltage vs current shows a linear behavior with coefficient of determination (R^2) between 0.9984-0.9999, where R is coefficient of correlation. The elements at the edges show higher output compared to other

elements as they also collect the charge in the guard ring region.

The attenuation of X-rays and consequently detection of transmitted photons has been studied by using different filters. The measured output voltage in each element for different filters in the path (Al, SS and Cu) and without filters is as shown in Fig.12. The mean value of the output voltage and the spread are: (i) No filter, 1.1 V \pm 0.2 V, (ii) Al filter, 0.86 V \pm 0.12 V, (iii) SS filter, 0.57 V \pm 0.09 V and (iv) Cu filter, 0.45 V \pm 0.04 V

The X-ray tube settings for these measurements were 140keV, 8mA. As expected the attenuation is more as the atomic number (Z) of the element is increased and therefore the output voltage in each element decreases as the filters are changed from Al to SS and to Cu.

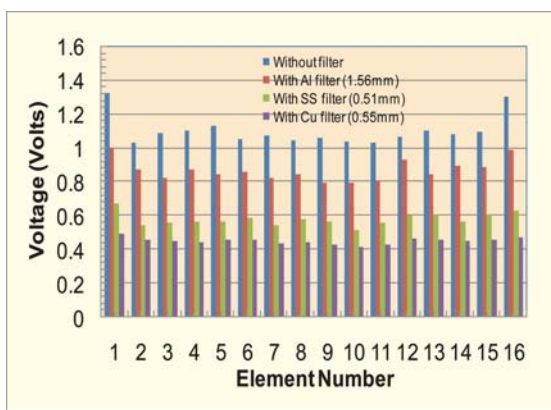


Fig. 12: Variation of output voltage of each element for no filter and with different filters

Summary

16-element CsI coupled photodiode linear array detectors suitable for X-ray baggage scanning applications have been indigenously developed. The X-ray performance of the CsI coupled photodiode detector has been studied using an X-ray source at BARC for different X-ray tube setting of 140 keV, 100 keV and 80 keV and for the current setting of 4 mA, 6 mA and 8 mA. The output voltage shows an expected dependence on tube voltage and current, i.e. linear dependence on current and square dependence on voltage. The total observed variation from element to element was within $\pm 7.5\%$. This variation includes several factors such as variation in photodiode, scintillator, optical coupling, etc. The linearity of the response was checked over a current range from 0.5 mA to 8 mA at 140 keV. All elements

show a linear dependence on current in this range. The performance study of the CsI-photodiode linear array detector with X-rays confirm the applicability of these detectors for X-ray baggage scanning applications. The technology developed for these arrays will be suitable for developing detectors for NDT applications such as X-ray tomography and security inspection system applications.

Acknowledgements

The authors would like to thank Shri G P Srivastava, Director, E&IG, Shri R K Patil, Associate Director (C), E&IG, Dr Gursharan Singh, Associate Director (I), RC&IG and Head, IAD for their support in carrying out this work. The authors are also thankful to Mrs Shruti Bhalekar, SA/E and Shri Bhavani P Singh, SA/D for their help in carrying out the experiments.

References

1. "Indigenous Development of Silicon PIN Photodiodes Using a 4" Integrated Circuit Processing Facility", Anita Topkar, Arvind Singh, Bharti Aggarwal, C.K. Pithawa and A S Rawat, *BARC NewsLetter*, Issue No. 318 Jan - Feb 2011, p 34-38.
2. S.G. Singh, Arvind Singh, Anita Topkar and S.C. Gadkari, "Performance of indigenously developed CsI(Tl)-photodiode detector for gamma-ray spectroscopy", AIP Conference Proceedings, 1349, (2011) p 481-482.

Marx Generator and Reflex Triode based High Power Pulsed Microwave Source

Archana Sharma, Amitava Roy, Sabyasachi Mitra,
Vishnu Sharma, S. Singh, Senthil Kumar,
Ankur Patel, Rakhee Menon, Ritu Agrawal,
A.K. Ray and D.P. Chakravarthy
Accelerator and Pulse Power Division

Abstract

A compact repetitive Marx generator and a High Power Microwave (HPM) source based on a matched reflex triode has been developed and tested. The Marx generator rated at 1 kJ, 300 kV, 12 kA, 10 Hz, is suitable to drive the reflex triode directly. Bipolar charging of the Marx generator has been used to get lower system inductance and consequently faster output rise time with relatively low charging voltage. Inductive charging of the Marx generator capacitors using a capacitor charging power supply has been used to make the system repetitive and enhance the system efficiency as compared to resistive charging. The Marx generator has been characterized using aqueous resistive load and the reflex triode vircator. Experiments have been conducted using the Marx generator and reflex triode system to generate intense relativistic electron beams and high power microwaves.

Introduction

High power pulsed sources have been employed for applications such as high power microwave (HPM) generation [1, 2], flash radiography [FXR] [3], and ion implantation for material modifications etc. Since 1970, BARC has indigenously developed many pulsed power systems such as KALI-75, KALI-200, KALI-1000, and KALI-5000 to generate intense relativistic electron beams for plasma heating and HPM generation experiments. (KALI is abbreviation of "Kilo Ampere Linear Injector"). HPM sources based on pulsed power systems are being used for applications in plasma heating, particle acceleration, high-power radar, and many other industrial and defense related fields. All the above mentioned 'KALI' systems are single shot systems. Marx generators are the most commonly used pulsed power sources. They are generally used in single shot devices for generating high voltages. Presently, there is a growing interest in the development of compact, repetitive pulsed power systems based on Marx generators for HPM generation. The compactness of Marx generator with its ability to

operate in repetitive pulsed mode has enhanced its appeal, when coupled directly to reflex triode, for HPM generation. It can be operated in both, positive and negative output polarities to drive reflex triode as well as axial and coaxial vircators. The Marx generator has the advantages of higher peak power rating, repetitiveness, compactness, low cost and reliability in comparison with the conventional pulse power systems such as pulse-forming networks (PFN), Tesla based systems and FCG generators.

The reflex triode is a member of the virtual cathode oscillator (vircator) family of narrow band radiation sources. Compared to other high power microwave sources like relativistic magnetrons, klystrons and Magnetically Insulated Line Oscillator (MILO), the vircator has a number of advantages like simple geometry, ease of operation and maintenance, does not need external magnetic field and virtually has no limit in power level of operation. A 1 kJ, 300 kV, 300 ns Marx generator and reflex triode have been developed for the generation of high intensity, high power electron beams and HPM.

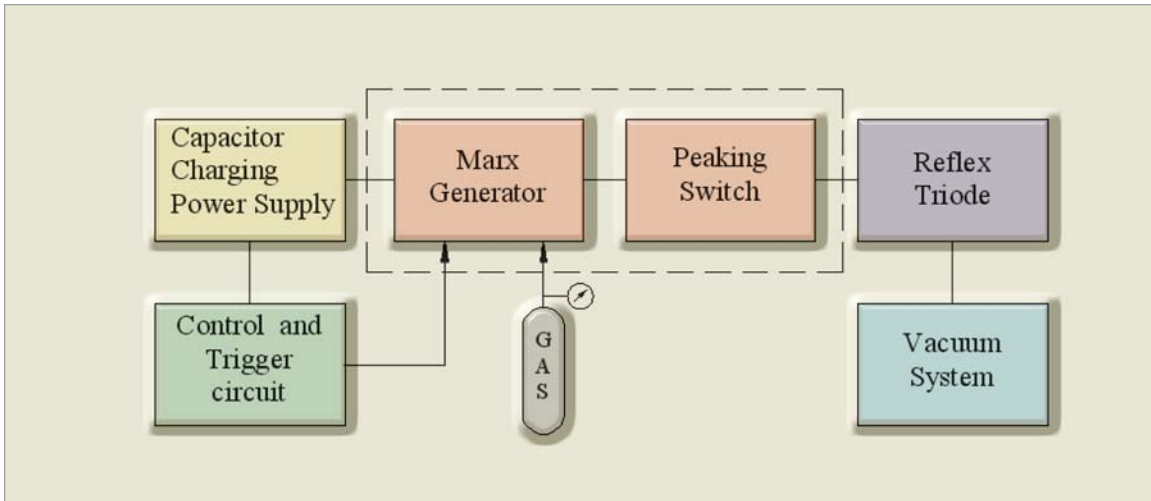


Fig.1: Block Diagram of a typical HPM system based on Marx Generator

System Description

The block diagram of a typical High Power Microwave system based on Marx generator is shown in Fig.1.

It consists of a high voltage dual capacitor charging power supply with negative and positive polarity outputs rated $\pm 40\text{kJ/s}$, Marx generator rated 1 kJ, 300 kV, 300 ns, 10 Hz, nitrogen gas supply system, spark gap based fast closing switch (peaking switch), reflex triode, vacuum system and control and trigger circuits. The trigger circuit based on IGBT switch and pulse transformer provides 10 kV pulse output to the first sparkgap switch of Marx Generator. The control circuit apart from setting charging voltage and repetition rate also provides synchronization of

the charging and trigger circuit during repetitive operation. Pulsed high voltages and currents are measured using aqueous CuSO_4 voltage divider (3000:1) and a self integrating Rogowski coil (10V/kA), respectively. High power microwave diagnostic systems based on receiving horn antenna and B dot probe are used to measure the radiated power and frequency.

1 kJ Marx Generator

A typical Marx generator scheme is shown in Fig. 2. Depending on the output voltage requirement, the Marx generator consists of a number of capacitors (C_0) charged in parallel to a voltage V_0 , through the charging resistor (R) and discharged in series through the spark gaps (S). The discharge

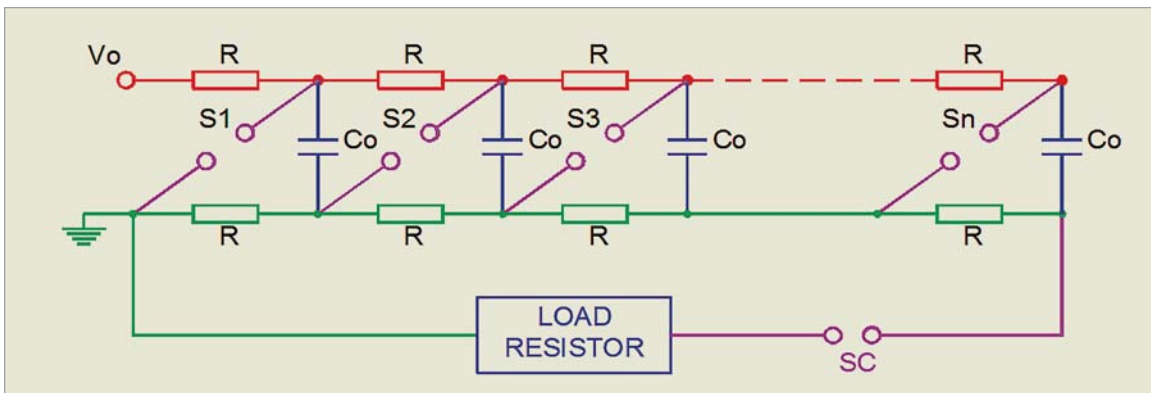


Fig.2: A typical Marx Generator scheme

is generally initiated by triggering the first one or more spark gaps by an external source. As a consequence the remaining gaps get over voltaged thus causing self breakdown. Such series discharge is generally referred to as erection of the Marx generator. The output closing switch (SC) is used to isolate the load while charging the Marx, and to ensure full Marx erection before energy is transferred to the load.

Resistive charging results in a large charging time and low repetition rate as compared to inductive type of charging of the capacitors [4]. Therefore in order to be able to operate at a repetition rate of 10Hz, the Marx generator was built with capacitor stages isolated by inductors and not resistors. During operation, as discussed above, the first switch (S1) is triggered, resulting in increase in the voltage across the remaining switches (S), causing a chain reaction of self-triggering. The six stages Marx generator is assembled from 12 capacitors (0.15 μ F, 50 kV each), 12 charging and isolating inductors (Lc+, Lc-, Lg: 100 μ H each) and 6 SS spark gaps [5, 6]. Fig. 3 shows the circuit diagram of the bipolar- and inductive-charging Marx generator.

The Marx generator configuration is based on bipolar charging to reduce the number of spark gaps as compared to unipolar charging, and also to have minimum possible inductance per stage. In bipolar Marx generator, half of the capacitors are connected

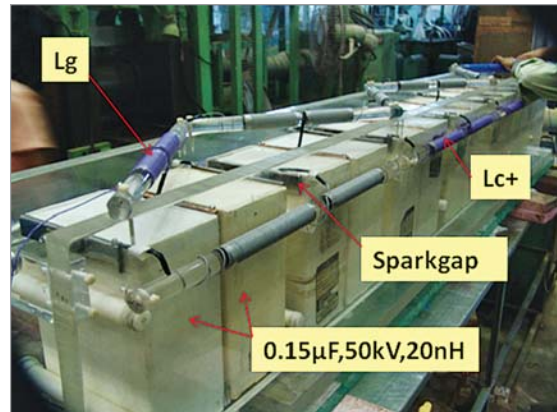


Fig.4: Internal assembly of Marx generator

to positive charging terminal and rest half are connected to the negative charging terminal through inductors. Connections are made such that all the capacitors get connected in series via spark gap switches during erection and discharge.

A photograph of the internal assembly of Marx generator is shown in Fig.4. Two stage prototypes of the Marx assembly were fabricated initially and experiments conducted to arrive at a layout which would provide lesser erected inductance and faster output voltage rise time. In the final assembly, the capacitors were mounted on 50 mm thick perspex sheets and sled into a SS chamber of 0.6 m inner diameter and length of 2 m. The Marx chamber was pressurized by nitrogen gas upto a maximum pressure of 3kg/cm². The assembled Marx generator with the closing switch and reflex triode is shown

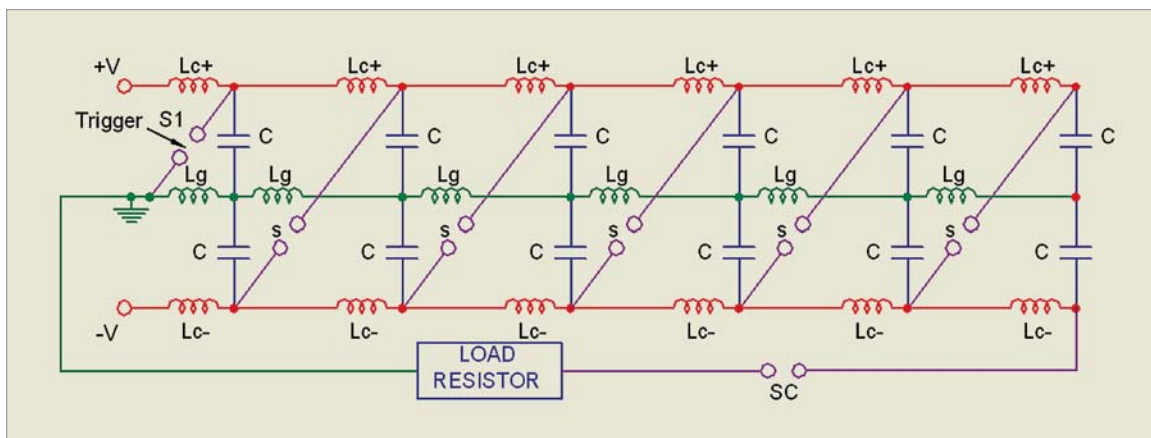


Fig.3: Circuit diagram of the bipolar charging Marx generator



Fig. 5: Photograph of 1kJ Marx generator with reflex triode

in the Fig.5. A fast (charging time: about 25ms) capacitor charging power supply was used to charge the Marx generator to a maximum voltage of 40 kV and at a maximum repetition of 10 Hz for burst mode operation.

Reflex Triode and HPM diagnostics

The reflex triode is a vacuum diode to generate intense electron beams by explosive electron emission process [7, 8]. It is housed inside a 400 mm dia. four way SS vacuum cylindrical chamber. An additional chamber is used to house the aqueous voltage divider and the Rogowski coil for measuring the diode voltage and current respectively. A vacuum pump is connected at the side port using a SS bellow and L-bend connection. The vacuum pumping system (Hind High Vacuum make Model: VS-250 D, capacity: 2000 ltrs/s) consists of a diffusion pump with liquid nitrogen trap backed by a rotary pump. A vacuum level of around 2×10^{-5} mbar is maintained in the reflex triode chamber during operation. Fig.6 shows the front view of reflex triode with vacuum pumping system. The vacuum seal on the top port is threaded to enable easy adjustment of the anode-cathode (AK) gap. The Marx output is connected to the anode of the reflex triode. The anode consists of a SS mesh, having 120 mm diameter and 70% transparency, fitted into a SS torus. The graphite cathode of 77 mm diameter is grounded.

A receiving horn antenna system consisting of a wideband ridged horn antenna, flexible ultra low



Fig.6: Front view of reflex triode with vacuum pumping system

loss cable (attenuation: 0.21dB/m at 2GHz and 0.26dB/m at 3GHz, length: 25 m), attenuators (40 dB), fast diode detector and an oscilloscope (1 GHz, 10 GS/s) is used to measure the peak radiated power signal. The HPM frequency and electric field measurement setup consists of a B-dot probe, flexible ultra low loss cable (25 m length) and a high band width oscilloscope (6 GHz, 40 GS/s).

System Performance

The Marx generator was tested initially with a matched 25 ohms aqueous CuSO_4 resistive load. The test results show a good agreement between estimated and measured parameters. At 12 kV charging, the measured peak output voltage is 100 kV. The system has been tested both in the negative and positive output polarity mode in repetitive burst mode operation and the overlapping waveforms of the output voltage recorded with 25 ohms CuSO_4 load at 10 Hz for 1 second, indicated an excellent repeatability (Figs. 7a and 7b).

Relativistic intense electron beam and high power microwave generation studies were conducted using the Marx generator and reflex triode system [9]. The AK gap was varied from 8 to 20 mm. It was found that the microwave power density and E-field peaked at 15 mm AK gap. Experiments on high power

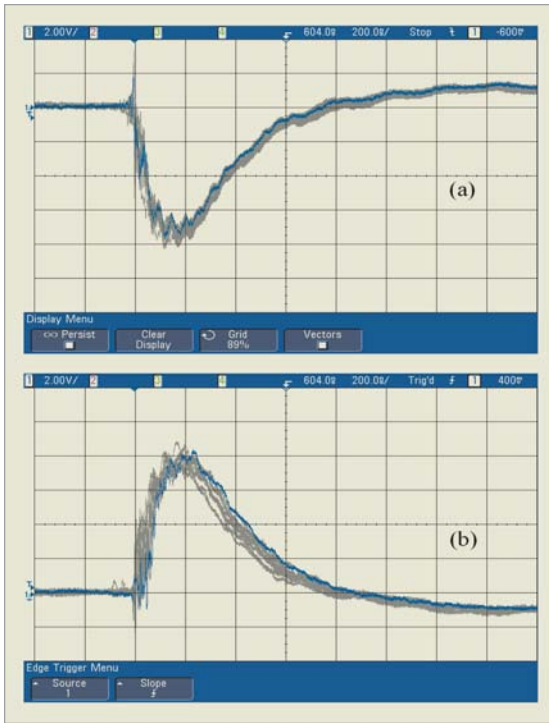


Fig.7: Marx output across 25 Ω resistive load for repetitive ten pulses (a) negative and (b) positive polarity (50 kV/div, 200 ns/div)

microwave generation were conducted for a fixed AK gap setting of 15 mm and Marx charging voltage set at 26, 35 and 40 kV. The HPM sensors were placed at a distance of 4.5 m which is in the far field region. (i.e. distance 'r' to be more than $2d^2/\lambda$ from the reflex triode window where 'd' is the diameter of the radiating window and 'λ' is the radiating wavelength). The receiving antenna kept in the far field will see a plane wavefront without phase difference across the receiving aperture. The electric and magnetic radiation fields (E and H) decay as 1/r and the radiation pattern is independent of 'r'.

The diode voltage, current and B-dot probe HPM signals and their FFTs are shown in Fig. 8.

The HPM electric fields measured using the B-dot probe at 4.5 m distance from the reflex triode window are about 9 kV/m, 14 kV/m and 5 kV/m at 26 kV, 35kV and 40kV Marx charging respectively. The HPM frequency measured was in S band and varied from 2.4 to 3.3 GHz depending on the Marx charging voltage. The free space radiation pattern

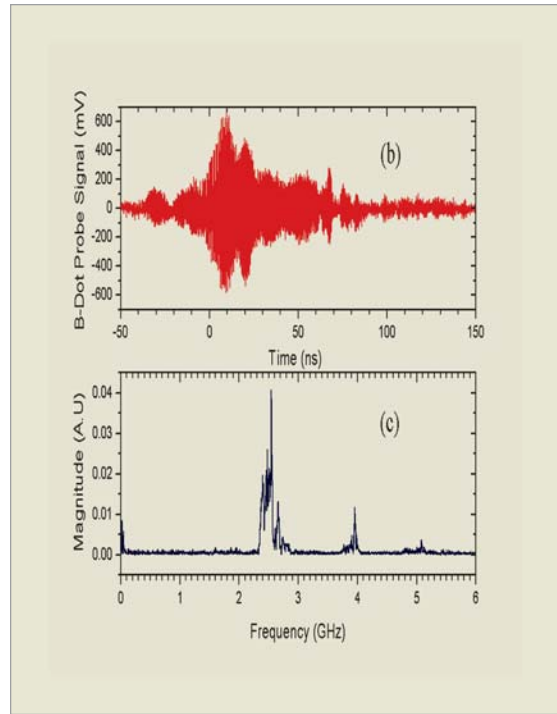


Fig. 8: For 15 mm AK gap and 26 kV charging (a) Diode voltage - current waveform (b) The B-dot probe signal and (c) its FFT

was plotted by varying the position of the B-Dot probe radially in the far field region, at a distance of 4.5 m from the reflex triode window and is shown in Fig.9.

All measurements were carried out keeping the anode plane horizontal, and varying the AK gap. Main radiation lobe was in the axial direction as shown in Fig. 9, indicating TE_{11} mode as the dominant mode of radiation. The gain (G_r) of the open ended wave guide of the reflex triode was estimated from the radiation pattern and was 4.35 dB [10]. The radiated power at the reflex triode was estimated using

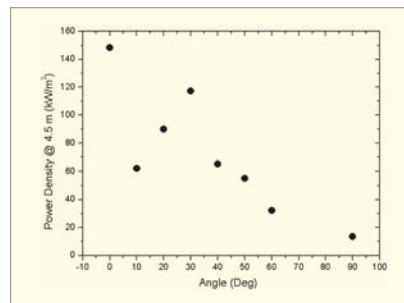


Fig.9: Measured radiation pattern on the horizontal plane

the radar equation [10]. The experimentally established peak HPM power generated at the reflex

triode was found to be 20 MW, 48 MW and 6.4 MW for charging voltages of 26 kV, 35 kV and 40 kV respectively at a fixed AK gap of 15 mm. The sudden drop in the microwave power at 40 kV charging voltage is attributed to the impedance mismatch between the Marx generator and the electron beam diode.

Conclusions

A compact repetitive high power pulsed microwave source based on a 1 kJ Marx generator and a reflex triode has been designed, developed and tested. The Marx generator has been tested in the repetitive mode with a matched resistive load and shows good repeatability. Subsequently, it has been used to drive a reflex triode for HPM generation. HPM has been generated by varying the anode-cathode gap of the reflex triode from 8 to 20 mm and charging voltages from 26 to 40 kV. The radiated HPM peak powers and electric fields have been measured using a diagnostic setup based on receiving horn antenna and B-dot probe. A maximum estimated peak power of 48 MW has been obtained at the reflex triode for 15 mm AK gap spacing and charging voltage of 35 kV. The radiated frequency was in the S band ranging from 2.4 GHz to 3.3 GHz. The radiation pattern indicated TE_{11} as the dominant mode of radiation.

Acknowledgement

The authors thank Dr. L. M. Gantayet, Director, Beam Technology Development Group, BARC for his constant encouragement and support. The authors would also like to thank Shri N. Lawangare, Shri S.P. Vaity and Shri S.G. Patil of APPD for their technical support.

References

1. E. H. Choi et al., "High-power microwave generation from an axially extracted virtual cathode oscillator," *IEEE Trans. Plasma Sci.* 28, (2000): 2128-2134.
2. S. H. Gold and G. S. Nusinovich, "Review of high-power microwave source research," *Rev. Sci. Instrum.* 68, (1997): 3945-3974.
3. Rakhee Menon, Amitava Roy, S. Mitra, A. Sharma, J. Mondal, K. C. Mittal, K. V. Nagesh, and D. P. Chakravarthy, "Generation and dose distribution measurement of flash x-ray in KALI-5000 system," *Rev. Sci. Instrum.* 79, (2008): 103301.
4. J. Lehr and C. Baum, "Charging of Marx Generators", Circuit and Electromagnetic System Design Notes, Note 43, Air Force Research Laboratory, Directed Energy Directorate, 29 June 2000.
5. A. Sharma, V. Sharma, D. D. P. Kumar, S. Mitra, K. Senthil, K. V. Nagesh, D. P. Chakravarthy, and A. K. Ray, "Experimental results on design aspects of a compact repetitive Marx generator," in Proc. IEEE Pulse Power Conference, Jun. 28, 2009.
6. Archana Sharma, Senthil Kumar, Sabyasachi Mitra, Vishnu Sharma, Ankur Patel, Amitava Roy, Rakhee Menon, K. V. Nagesh, and D. P. Chakravarthy, "Development and Characterization of Repetitive 1-kJ Marx-Generator-Driven Reflex Triode System for High-Power Microwave Generation," *IEEE Trans. Plasma Sci.* 39, (2011): 1262- 1267.
7. J. Benford, J. A. Swegle, and E. Schamiloglu, *High Power Microwaves*, Second Edition, Taylor & Francis, 2007. ISBN 0-750-30706-4.
8. G.A. Mesyats, *Pulsed Power* (Kluwer Academic/ Plenum Publishers, New York, 2005), ISBN 0-306-48653-9.
9. Amitava Roy, Archana Sharma, Sabyasachi Mitra, Rakhee Menon, Vishnu Sharma, K. V. Nagesh, and D. P. Chakravarthy, "Oscillation Frequency of a Reflex-Triode Virtual Cathode Oscillator," *IEEE Trans. Electron Devices* 58, (2011): 553 – 561.
10. Limin Li, Lie Liu, Guoxin Cheng, Qifu Xu, Hong Wan, Lei Chang, and Jianchun Wen, "The dependence of vircator oscillation mode on cathode material," *J. Appl. Phys.* 105, (2009): 123301.

Technology Transfers from BARC

“Lascan Dia Gauge” technology

The technology of “LASCAN DIA-GAUGE” has been developed by Laser & Plasma Technology Division, BARC. This technology use optical technique which is simple, cost effective and accurate. It is based on the beam scanning principle. It uses low power Laser diode as light source. The beam intensity and collimation properties of Laser are useful in design of the system while its wavelength (670nm) is useful during alignment. The instrument can measure the

diameters of transparent as well as opaque object in the range of 1 mm to 25mm with an accuracy of ± 5 micron. No warm up time required. The software offers facility for selection of samples by setting diameter range of user’s interest. Its microcontoller based circuit calculates and displays diameter upto 3rd decimal place in mm on LCD.

The know-how has been transferred to M/s Kraft Engineers, Mumbai on 22nd March, 2012.



Photograph after signing the agreement with M/s Kraft Engineers, Mumbai, seen from left to right Smt. S. S. Murudkar, TT&CD, Shri V. K. Upadhyay, TT&CD, Dr. S. P. Kale, Head, TT&CD, Smt. Varsha Mehta & Shri Hasit Mehta, Director “Rollotech Systems Pvt Ltd”, Dr. A. K. Das, Head, L&PTD, Dr. A. S. Rawat, L&PTD, Dr. S. S. Thattey, Head, LE&AS, L&PTD, Shri. N. O. Kawade, L&PTD.

The know-how of the following three water related technologies were transferred to M/s Mahavir Pumps Manufacturing Pvt. Ltd., Kolkata on 28th March, 2012.

i) On-line domestic water purifier based on ultrafiltration polysulfone membrane” technology.

The technology of “On-line domestic water purifier” has been developed by Desalination Division, BARC.

This device is based on polysulfone type of ultrafiltration membrane, which coated on a unique cylindrical configuration. This device on connecting to domestic tap purifies the domestic water with respect to microorganism, colour, odour, suspended

solids and organics. It is very effective as it removes bacteria to the extent of > 99.99% (4 log scale) & removes complete turbidity and produces crystal clear water. This device does not need electricity or addition of any chemical. It is almost maintenance free except occasional cleaning of suspended solids which deposit on membrane surface and this does not take more than few minutes.

It produces about 40 liters of pure water per day at about 5 psig head and works from 5 psig to 35 psig. The device filters out bacteria, no dead bacteria in the final filtered water. (All the raw materials required are produced within the country and are available locally).

ii) “Membrane Assisted Defluoridation Process for Safe Drinking Water” technology:

The technology of “Membrane Assisted Defluoridation Process for Safe Drinking Water” has been developed by Desalination Division. The ultrafiltration membrane assisted sorption process for removal of fluoride from ground/surface water provide safe drinking water and solves the serious problem of aluminium contamination in the product

water coming after defluoridation unit, which is more harmful than fluoride. The process provides safe drinking water not only free from fluoride but also free from secondary contaminants like aluminium and microorganisms. It can be adopted at both domestic and community level with/without the use of electricity.

iii) “UF Membrane Assisted Device for removal of Iron from contaminated water for drinking purposes” technology:

The technology of “UF Membrane Assisted Device for removal of Iron from contaminated water for drinking purposes” has been developed by Desalination Division. Iron is not considered hazardous to human health in moderate levels. In fact, iron is essential for good health because it facilitates transportation of oxygen in blood. However, when the level of iron in water exceeds 0.3 mg/l (ppm) limit, people experience red, brown, or yellow staining of laundry, glassware, dishes and household fixtures such as bathtubs and sinks. The water may also have a metallic taste and an offensive odour. Consumption of water with excess iron



Photograph after signing the agreement with M/s Mahavir Pumps Manufacturing Pvt. Ltd., Kolkata, seen from left to right Shri B. K. Pathak, Head, IPMS, TT&CD, Shri Susil Teewari, MTS, DD, Dr. P. K. Teewari, Head, DD, Dr. S. P. Kale, Head, TT&CD, Shri Praveen Kumar Poddar, Director, M/s Mahavir Pumps Manufacturing Pvt. Ltd., Kolkata, Shri D. Goswami, Head, MTS, DD, Dr. R. C. Bindal, Head, MDS, DD, Shri Soumitra Kar, MDS, DD, Shri V. K. Upadhyay, TT&CD.

causes constipation accompanied by other physiological disorders. UF membrane assisted oxidation process for removal of iron from ground/surface water makes it safe for drinking purposes. It is a simple, cost effective, process adaptable at both domestic and community level and is capable of dealing with high levels of iron contamination.

The technologies of UF membrane device used in this process are already available at domestic level (Dead-end element type) and at community level (Back washable flow element type) as separate technologies with BARC.

“Membrane Assisted Defluoridation Process for Safe Drinking Water” technology:

The technology of “Membrane Assisted Defluoridation Process for Safe Drinking Water” has been developed by Desalination Division. The ultrafiltration membrane assisted sorption process for removal of fluoride from ground/surface water provide safe drinking water and solves the serious problem of aluminium contamination in the product water coming after defluoridation unit, which is more harmful than fluoride. The process provides safe

drinking water not only free from fluoride but also free from secondary contaminants like aluminium and microorganisms. It can be adopted at both domestic and community level with/without the use of electricity.

The know-how has been transferred to M/s Waterlife India Pvt. Ltd., Secunderabad on May 18th, 2012



Photograph after signing the agreement with M/s Waterlife India Pvt. Ltd., Secunderabad, seen from left to right Smt. S. S. Murudkar, TT&CD, Shri V. K. Upadhyay, TT&CD, Shri Jai Dutt Sharma, Head- Technical, M/s Waterlife India Pvt. Ltd., Secunderabad Dr. P. K. Teewari, Head, DD, Dr. S. P. Kale, Head, TT&CD, Shri Kumar Priya Ranjan, Director, Waterlife India Pvt. Ltd., Secunderabad, Dr. R. C. Bindal, Head, MDS, DD, Shri Soumitra Kar, MDS, DD.

BRNS-AEACI Third School on Analytical Chemistry (SAC-3): a Report

Third School on Analytical Chemistry (SAC-3) sponsored by the Board of Research in Nuclear Sciences (BRNS) was jointly organized by Association of Environmental Analytical Chemistry of India (AEACI) and Department of Chemistry, Sri Krishnadevaraya University (SKU) at, SKU, Anantapur, Andhra Pradesh during February 24 – March 01, 2012. A total of 60 young academics, research scholars from Universities and budding scientists from different DAE units participated in this school. The inaugural function was held at Phule Bhavan, S.K. University on 24th February 2012 and Prof. Buddanna, Principal, SKU presided over the inaugural function. Prof. K. Ramakrishna Reddy, Vice Chancellor, S.K. University inaugurated the school. Dr. T. Mukherjee, Director, Chemistry Group, BARC and Chairman, National Advisory Committee, SAC delivered the key note address. Prof. T. Sreenivasulu Reddy, Convenor, Local Organising Committee, SAC-3 welcomed the guests

and the participants. Dr. A.V.R. Reddy, Chairman, Technical Committee, SAC and Head, Analytical Chemistry Division, BARC explained the theme of the school and spoke on the importance of practical training and continuous education that SAC aims to provide. He stressed that the SAC's provide a good opportunity for both the participants and the resource persons to learn from each others' experience and expertise thus facilitating collective growth of the analytical chemistry fraternity. Prof. Ramakrishna Reddy, Vice Chancellor in his presidential address expressed his happiness to be associated with SAC-3 and spoke on the importance of Chemistry, and particularly analytical chemistry. Later, he released a practical book entitled "Experiments in Analytical Chemistry" authored by A.V.R. Reddy, K.K. Swain and K. Venkatesh. Dr. Mukherjee in his keynote address emphasised the importance of Good Laboratory Practices in generating high quality and reliable analytical data.



(L-R) Prof. Buddanna, Dr. A.V.R. Reddy, Dr. T. Mukherjee, Prof. K. Ramakrishna Reddy, Prof. T. Sreenivasulu Reddy and Prof. L.K. Ravindranath at the book release event

He stressed that due attention must be paid to safety and safe practices while carrying out laboratory work. Prof. L.K. Ravindranath, Secretary, Local Organising Committee proposed a vote of thanks.

The school schedule consisted of lectures in the morning sessions and laboratory experiments in the post-lunch sessions. The morning lecture sessions provided the participants a platform to listen to lectures delivered by eminent people in the field of analytical chemistry. The topics covered were QA/QC, accreditation, neutron activation analysis, environmental monitoring & remediation, chromatographic techniques, thermal analysis, spectrophotometric techniques like ICP-OES & AAS, Electroanalytical techniques and elemental speciation in analytical chemistry. Lectures were delivered on statistical treatment of data and use of spreadsheets in analytical chemistry. Additionally, three special lectures on; 'Mass Spectrometry and Applications' by Prof.(retd.) C.D. Reddy, S. V. University, Tirupati, 'Exploration Techniques for Atomic Minerals and Future Strategies' by Dr. P.S. Parihar, Director, AMD and 'Transition from Laboratory reactions to Industrial Production' by Shri S.K. Ghosh, Director, Chemical Engineering Group, BARC were arranged.

The participants had hands-on training on five experiments that were carried out in five batches on rotation basis. The experiments were (1) Multi element determination using absorption spectrometry, (2) Thermal studies of oxalates, (3) Determination of toxic elements by cyclic voltammetry, (4) Analysis of gaseous samples and particulate matter for environmental monitoring and (5) Analysis of COD, BOD & fluoride in waters and waste water sample. Besides demonstration experiments on HPLC, IR spectroscopy and Bomb calorimeter, the laboratory experiments generated a lot of interest among the participants, S.K. University scholars and also the local press.

On the penultimate day of the school, seminar presentations by each of the five experimental groups were held. 'Frontiers in analytical chemistry' was the general theme for seminar presentations and a topic was assigned to each group three days earlier. The seminar gave a unique opportunity to the participants to work collectively in groups with diverse knowledge and experience which was a mutually benefiting experience. One member from each group delivered the seminar and the remaining members participated in the lively Q & A session after the seminar presentation. On the final day of the school an objective type written examination on the topics covered during the school was held for the participants and all the participants have done reasonably well. In an interactive feedback session, participants expressed their views and most of them felt that the lectures were excellent and the laboratory experiments were arranged thoughtfully. They also felt that smaller groups for laboratory experiments would have been better.

Valedictory function held on March 01, 2012 and Prof. Rajarami Reddy, Vice Chancellor, V. S. University, Nellore was the chief guest and was chaired by Prof. P.L.N. Reddy, Coordinator, Sai Baba College, Anantapur and former EC member, S.K. University. Prof. T.S. Reddy welcomed all to the valedictory function. Dr. A.V.R. Reddy gave the gist of the technical feedback and thanked the organizers for conducting the School. Prof. Ramakrishna Reddy in his presidential address appreciated the efforts of local organisers and profusely thanked AEACI, BRNS and BARC for conducting the School in S.K. University. Prof. Rajarami Reddy explained the importance of Analytical Chemistry and the possible impact of such a School. Prof L.K. Ravindranath gave a gist of the feedback. Awards were given to the best group seminar presentation and to the top five rankers in the written examination by Shri P.L.N. Reddy. He also distributed participation certificates. Shri K. Venkatesh, BARC proposed a vote of thanks.

Technology of Indigenous Digital Radiotherapy Simulator Transferred

Radiotherapy Simulator is useful to diagnose the physical extent of the tumor and its relation to the surrounding tissues for proper selection of the size and orientation of the radiotherapy beams for the treatment of localized cancers. It helps to plan the radiotherapy treatment while avoiding exposure to the critical organs in the beam-bath and limiting the exposure to the healthy tissues/organs adjacent to the tumor to be treated.

It is similar to an isocentric external beam therapy machine. However, it uses diagnostic X-ray beams for imaging, either in radiography or in fluoroscopy mode. The capability of real-time acquisition and analysis of the digital images helps in fast, accurate treatment planning and verification.

Considering the growing need for such machines in our country, the Division of Remote Handling & Robotics (DRHR) of BARC has successfully developed the technology. The first unit is commissioned successfully at Indian Red Cross Society Hospital, Nellore, AP.

The technology is transferred to M/s. Panacea Medical Technologies Pvt. Ltd., Bangalore for commercialization of the machine. An agreement between BARC and M/s Panacea has been signed accordingly on 16th Nov. 2011. The Technology Transfer and Collaboration Division (TT&CD) of BARC coordinated the activities associated with this transfer.



Sitting (L-R): Dr. N. Khalap (TT&CD), Ms. S. S. Mule (TT&CD), Dr. I. Ravi, Dr. R. K. Sinha, Director, BARC, Manjit Singh (Director, DM&A Group, BARC and Head DRHR), A. M. Patankar (Head, TT&CD). Standing (L-R): Dr. D. C. Kar (DRHR), R. V. Sakrikar (DRHR) and R. Sahu (DRHR).

Graduation Day Function of the BARC Training School; a Report

The Graduation Day function of OCES 2011 and OCDF 2011 batches of the BARC Training School, Mumbai, was held on 30th July, 2012 at the Central Complex Auditorium, BARC. 115 Graduates from 12 science and engineering disciplines received the OCES certificates along with 18 graduates of the OCDF stream.

The Chief Guest for the function was His Excellency Shri M.K.Narayanan, Hon'ble Governor of West Bengal. The function was presided over by Dr R.K.Sinha, Secretary DAE and Chairman AEC. Shri Sekhar Basu, Director BARC delivered the welcome address in which he reminded the trainees about the great training school legacy going back 55 years and asked them to put in their best effort in the years to come. Dr R.K.Sinha, in his presidential address brought out the challenges and opportunities that the Department provides for these young trainees and wished them success in their future endeavours. Shri M.K. Narayanan in his address traced the journey of DAE and the important role it has to play in the years to come- both in the energy and strategic sectors.

The first rankers in each of the 13 disciplines were conferred the prestigious Homi Bhabha Prize, which comprises a Homi Bhabha Medal, a certificate and a cash prize. The medals and certificates were received by the proud recipients at the hands of the



His Excellency Shri M.K.Narayanan, Hon'ble Governor of West Bengal. addressing at the function

Chief Guest. All OCES and OCDF trainees went on to receive the Graduation Certificates at the hands of Director, BARC.

Mementoes were presented to the Chief Guest by Chairman. AEC and Director, BARC.

Dr. R.R.Puri, Head HRDD and Dean, HBNI delivered the vote of thanks in which he emphasised upon the stellar role of the training school faculty in carrying forward the great tradition of the BARC training school. He took the opportunity to thank all wings of the BARC administration whose support is invaluable in carrying out the programs of the BARC Training School.

The National Anthem was rendered by the gathering to bring the event to an end.



First rankers in each of the 13 disciplines with the Chief Guest His Excellency Shri M.K.Narayanan, Hon'ble Governor of West Bengal. To his right: Shri Sekhar Basu, Director BARC, left: Dr R.K.Sinha, Secretary DAE and Chairman AEC, Dr. R.R.Puri, Head HRDD and Dean, HBNI.

National Fire Service Week at BARC: a Report

Every year, 14th April is observed as National Fire Service Day. On this day in the year 1944, fire service personnel displayed exemplary courage and devotion to duty as they fought the major devastating fire that had erupted following an explosion on a Ship S.S. Fort Stikine berthed at the docks of Mumbai Port Trust. Many fire fighters lost their lives, leaving behind their names etched in the minds of Mumbaites forever.

Several programmes were organized by the Fire Service Section (FSS), BARC during the Fire Service Week April 14-20, 2012, to create fire safety awareness among the employees in BARC, Trombay and the residents of Anushaktinagar. On behalf of BARC, Shri A.K. Tandle, Chief Fire Officer placed wreaths on the 14th of April at the memorials erected on the grounds of Mumbai Port Trust and at the headquarters of Mumbai Fire Brigade, Byculla. On 15th April, BARC FSS team participated in the three-man hose drill competition arranged by Mutual Aid Response Group, Trombay-Chembur Industrial Belt and secured the 1st prize. Ten other teams belonging to various industries participated in the competition. A film on "Preventing Accident in the Home" was screened through the cable network at Anushaktinagar. On 16th April, two crews from BARC FSS participated in Tactical Medley Drill Competition organized by the Govt. of Maharashtra at Cross Maidan, Dhobi Talao, Mumbai. 18 teams belonging to various organizations participated in the competition. Mumbai Fire Brigade stood first with 38.74 seconds, BARC stood second with 38.84 seconds. In another event of Individual Ladder Drill, Pune Fire Brigade stood first with 14.03 seconds and BARC stood second with 14.07 seconds. On 17th April, Dr. R.K. Sinha, Director, BARC was offered a pin flag to inaugurate the fire service week and start the fund raising campaign. Pin flags were also offered to Shri S.G. Markandeya, Controller, BARC, Shri S.K. Ghosh, Director, Chem. Engg. Group and Shri Hanmanth Rao, Head, ChED. A one act play on fire safety was arranged for BARC employees at the Central Complex Auditorium. Director, Chem.



Shri A. K. Tandle, Chief Fire Officer, BARC offering Pin Flag to Dr. R. K. Sinha, Director, BARC on the occasion of the Fund Raising Campaign

Engg. Group and Controller, BARC, addressed the gathering before the One act play. Head, Personnel Division, CAO, Director, Security (S & C) were also present during the programme. On 18th April, BARC FSS team participated in a Volleyball competition arranged by MARG and secured 2nd prize. Seven other teams from various industries from Chembur participated in the event. A programme on Fire Fighting Equipment Exhibition with fire fighting and rescue demonstration was also organized at the Dhruva Premises. On 19th April, a live Fire Fighting and Rescue Demonstration was organized at BARC Hospital, Anushaktinagar. Around 300 people including doctors, matrons and hospital staff witnessed the programme. On 20th April, a prize distribution function was arranged at the Fire Station, BARC for the winners of various competitions conducted among BARC fire service personnel. Shri Hanmanth Rao, Head, ChED distributed the prizes to the winners. This year an amount of Rs.14,744/- was collected through cash donations during Fire Service Week Observance – 2012. The Fire Service Week culminated on 20th April, with a ceremonial parade at Cross Maidan, Dhobi Talao, Mumbai in which BARC's Fire Service personnel contingent participated with Emergency Rescue Tender and equipment. Hon'ble Shri J.K. Sinha, Member, National Disaster Management Cell chaired the concluding function.

Release of BARC Logo and Launching of an Enhanced Website for BARC: a Report

On 10th August, 2012, Shri Sekhar Basu, Director, BARC released a logo for BARC and also launched the BARC website in its new, enhanced version. The event was organized by the Scientific Information Resource Division, (SIRD), BARC. Speaking on the occasion, the Director said, that the release of 'BARC Logo' was a historic moment for all of us in BARC. He also that it was a matter of great pride to have a unique identity for BARC which symbolizes the whole spectrum of it's R & D activities, it's mandate and objectives. He acknowledged the contribution of Dr. R. K. Sinha, Chairman, AEC who was closely associated with the development of the logo through various stages. He described the significance of every component of the logo. He also felicitated the faculty of the Industrial Design Centre, IIT Bombay, Mumbai for designing the BARC logo. He thanked everyone who was involved in making the logo a reality, including SIRD, which coordinated the entire activity. He called upon all the scientific community to extensively use the logo in their presentations in National and International fora.

Shri G. P. Srivastava, Director, E & I Group, BARC welcomed the gathering. In his welcome address, he said that a logo creates a long lasting impression on people, expresses the aims and objectives of the organization and provides a point of recognition to all the people working in the

organization. He concluded by saying that releasing of the BARC logo was a moment to be cherished in the history of BARC.

Shri S. G. Markandeya, Controller, BARC made a presentation on how the logo could be used on letterheads, visiting cards, identity cards, Power Point presentations, vehicles, stationary items etc. He also presented certificates to the three shortlisted finalists of the BARC logo design competition which was organized by SIRD.

Dr. K. Bhanumurthy, Head, SIRD, gave an overview of the enhanced BARC Website with various special features such as the AHWR Critical Facility, R&D activities, Public Awareness Programmes, Visitors Corner, Students Corner, Career opportunities in BARC etc. Shri Manoj Singh, SIRD proposed the vote of thanks.



Shri Sekhar Basu, Director, BARC, speaking on the occasion of the BARC logo release and launching of enhanced BARC website

Nuclear Energy and Development of Country (NEDC – 2012): a Report

A two-day symposium on “Nuclear Energy and Development of Country (NEDC – 2012)” was organized by the BARC Employee’s Association, Tarapur (BARCEAT) in association with the Board of Research in Nuclear Sciences (BRNS), Mumbai on 25th and 26th of August, 2012. The aim was to spread awareness about Nuclear energy and its applications with an objective to enlighten the people at Tarapur, with the different areas in which nuclear energy is being used for the benefit of society. BARCEAT has already taken a lead in involving Heads of local villages (Sarpanch), Principals and educationists from local schools and colleges apart from senior employees of the DAE family to further this aim. Shri. S. Basu, Director BARC inaugurated the symposium in the presence of Dr. G.J. Prasad, Director, Nuclear Fuels Group, Shri Ravindranath, Site Director, Tarapur Maharashtra Site, Md. Afzal, Director GSO and Head, AFFF, Shri H.T. Raut, President BARCEAT, and Shri J.H. Raul, General Secretary BARCEAT. Director BARC appreciated the efforts of BARCEAT in educating the villagers/ society about the usefulness of nuclear energy for societal benefits and the safety precautions being taken during all operations. About 600 delegates participated in the deliberations.

Invited talks from experts in different areas of nuclear energy were arranged during the symposium. Considering the participation of villagers, Principals and educationists from local schools and colleges almost all the talks were in local language Marathi as well as in Hindi. Dr. S.K. Malhotra, Head, Public Awareness Division, DAE, BARC, Mumbai described the need for nuclear energy for social benefits as well as for national progress. Dr. Gursharan Singh, Associate Director, RC & IG elaborated on the “Societal Applications of Isotope / Radiation Technology in Industry and Hydrology”. Dr. S.G. Bhagwat, NABTD, BARC, Mumbai spoke on

“Nuclear Techniques in Agriculture”. He briefly described about the various high yielding and high insect resistant species of food grains and emerging utilization of food irradiation technology to increase the shelf life of various food items like onion and potato. Dr S.P. Kale, TTCD, BARC, Mumbai spoke on the various agricultural problems.

Shri V.K. Savarkar, GM, NRB briefed about the energy security for the country. Dr. S.V. Thakre, Radiopharmaceuticals Division, discussed about the production of various radioisotopes required for nuclear medicine. Dr. Puroshottam Kand, RMC explained in a very simple language about how nuclear medicines are good diagnostic tools and the use of various nuclear medicine for treatment of certain diseases. Dr. M.S. Daniel, TAPS Hospital explained about the misconceptions associated with radiation in a talk on “Health Profile of Employees of NPCIL – A Retrospective Analysis (1995 – 2010)”.

Shri D.D. Akre and Chandrakant Salunke from TAPS 1 – 4 briefly gave an introduction to application of nuclear energy for power generation and described about the safety of the Nuclear power plants at Tarapur. Shri P.G. Behere, Plant Superintendent, AFFF described the MOX fuel fabrication at Advanced Fuel Fabrication Facility, Tarapur. Shri Saurabh Garg elaborated about IERMON for environmental radiation monitoring. Dr. N.L. Sonar, TWMP, NRB explained about various waste management practices being followed for different types of radioactive wastes at Tarapur. Dr. Amrit Prakash Superintendent, Quality control section of AFFF briefly outlined about Nuclear Energy and Radiation. Shri U.V. Deokar, Radiation Safety Officer, TWMP described the basic concepts of Radiation and its measurement / monitoring.

The symposium concluded with a feedback session from participants of nearby villages.

BARC Scientists Honoured

Name of the Scientist	: Sudhakar Srivastava Nuclear Agriculture & Biotechnology Division, For his research work in the field of Biological Sciences
Award	: NASI Young Scientist Platinum Jubilee Award
Presented at	: The National Academy of Sciences, India (NASI) at Allahabad on Nov. 26, 2011
<hr/>	
Name of the Scientists	: Sudha Premachandran; Nazir M.Khan, Vikas S.Thakur, Jyoti Shukla and T.B.Poduval. Radiation Biology & Health Sciences Division
Title of the paper	: Differential immunotoxic effects of ethanol on murine EL-4 lymphoma and normal lymphocytes is mediated through increased ROS production and activation of p38MAPK.
Award	: ABAP Young Scientist Award.
Presented at	: International Symposium on Innovations in Free Radical Research and Experimental Therapeutics (IFRRET-2011) and 5th Annual Convention of Association of Biotechnology and Pharmacy (ABAP) held at Coimbatore from December 7-9, 2011
<hr/>	
Name of the Scientists	: Rohit Shukla, Surender Kumar Sharma, Partha Bannerjee, Pankaj Deb, T. Prabakaran, Rashmita Das, Basanta Das, Biswajit Adhikary, Rishi Verma and Anurag Shyam Energetics & Electromagnetics Division
Title of the paper	: Microwave Emission from a AXIAL-Virtual Cathode Oscillation Driven by Compact Pulsed Power Source
Award	: Best Poster Award and a Cash Prize of Rs. 5000/-
Presented at	: International Symposium on Vacuum Science & Technology and its Application for Accelerators -2012, VECC Kolkata, during 15-17 February, 2012.



V. R. Chavan
Wooden Art Work

Edited & Published by:
Dr. K. Bhanumurthy,
Head, Scientific Information Resource Division,
Bhabha Atomic Research Centre, Trombay, Mumbai 400 085, India
Computer Graphics & Layout: N. Kanagaraj, SIRD, BARC
BARC Newsletter is also available at URL:<http://www.barc.gov.in>